Thin-Walled Structures 180 (2022) 109857

Contents lists available at ScienceDirect

Thin-Walled Structures

journal homepage: www.elsevier.com/locate/tws

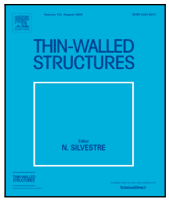

Full length article

Free and forced small flexural vibrations of slightly curved slender composite beams with interlayer slip

Christoph Adam *, Dominik Ladurner, Thomas Furtmüller

Unit of Applied Mechanics, University of Innsbruck, Technikerstr. 13, 6020 Innsbruck, Austria

ARTICLE INFO

Keywords:
Imperfect beam
Flexible bonding
Layered beam
Natural frequencies
Slightly curved beam
Initial deflection

ABSTRACT

This paper presents a beam theory for analyzing the dynamic bending response of slender slightly curved composite beams whose layers are flexibly connected and therefore subject to interlayer slip. The equations of motion and boundary conditions are derived using Hamilton's principle, assuming separately for each layer the applicability of Euler–Bernoulli theory and a linear elastic relationship between the interlayer slip and the shear traction. For the problem of a three-layer slightly curved single-span beam with symmetric layer arrangement and soft-hinged bearings, analytical expressions for the natural frequencies and the eigenfunctions are derived. For the arbitrarily supported two-layer beam, on the other hand, a numerical solution scheme of the combined initial boundary value problem is presented. Several examples show how important it is to consider even very small deviations from the straight beam axis in the prediction of the dynamic response for slender beams with interlayer slip, in particular when all supports are immovable. The comparison of the beam solutions with the results of much more expensive FE analyses based on plane stress elasticity proves the accuracy of the presented theory.

1. Introduction

Layered structural members such as beams, plates and shells consist of several layers of different materials that are joined together. If the flexibility of the fasteners (e.g. adhesives, bolts and nails) is very low, then the layers are assumed to be rigidly bonded. However, very often the connection of the layers is flexible, which results in relative displacement of the layers at the interfaces when a load is applied, which is referred to in the literature as interlayer slip. In composite members with flexibly bonded layers, the mechanical behavior is more complex than in homogeneous members. This has been recognized for a long time and corresponding theories have been developed in the past for the analysis of composite beams with interlayer slip.

As examples of many publications on the structural analysis of layered beams with flexible bonding, the papers [1–3] are mentioned here. In a recent paper [4] even the rotational stiffness of the interface between two layers, modeled according to Timoshenko theory, was taken into account. In a more elaborate approach, [5] solved the Airy stress function for the two-layer beam with interlayer slip assuming a plane stress distribution. Investigations on buckling of beam columns with interlayer slip can be found, for instance, in [6,7]. In addition, numerous research efforts have been made to model the geometric and material non-linear behavior of beams with interlayer slip [8–10]. Several studies are also concerned with predicting the dynamic response of composite beams with flexible bonding, such as [11–17].

In all these studies it is assumed that the beam axis is straight. In reality, however, the member axis is almost always curved, either due to an unintentional imperfection or intentionally. Depending on the scale and boundary conditions, such initial deflection can have a major impact on the response of the structural member. Accordingly, there are many papers in which corresponding theories have been proposed to predict the response of curved beams. These papers refer either to homogeneous beams (e.g. [18–20]) inhomogeneous beams (e.g. [21–23]) or layered beams with rigid bonding (e.g. [24–29]). In this context, some studies on the dynamic behavior of shells and curved panels should also be mentioned [30–38]. A review on vibrations of curved (and straight) layered beams can be found in [39]. However, to the authors' knowledge only the study by Lengyel [40,41] exists for the static analysis of composite beams with deep curvature and interlayer slip. For slightly curved beams, a first paper on the static analysis of moderately large deflections of such layered members with flexible bonding has been published only recently [42]. The *dynamic response* of curved laminated beams with interlayer slip has not been investigated at all so far.

To fill the gap, this paper presents a beam theory for the analysis of linear free and forced small vibrations of slightly curved composite beams with elastically bonded layers. This theory is based on a layer-wise application of the Euler–Bernoulli theory as well as linear elastic material behavior. After establishing the basic kinematic relations and

* Corresponding author.
E-mail address: christoph.adam@uibk.ac.at (C. Adam).

https://doi.org/10.1016/j.tws.2022.109857
Received 29 January 2022; Received in revised form 15 June 2022; Accepted 18 July 2022
Available online xxxx

the force and moment resultants for a three-layer beam, the equations of motion and the corresponding boundary conditions are derived by means of Hamilton's principle. Slender beams in the low frequency range are considered, thus shear deformation, rotational inertia and longitudinal inertia are neglected. For a soft-hinged three-layer beam with symmetric layer structure, analytical expressions for the natural frequencies and eigenfunctions are found. The difference in the modal parameters between the horizontally immovably supported slightly curved beam and the beam with one horizontally sliding support is elaborated. The free and forced vibration of a slightly curved two-layer beam with arbitrary boundary conditions, on the other hand, is determined approximately by applying the Galerkin method. The modal parameters found with this beam theory and the vibration response of application examples are contrasted with results from comparative finite element (FE) analyses on numerical models based on a plane stress state to show the accuracy of the proposed theory.

2. Basic equations

A layered beam of length l under plane bending is considered, for which the following assumptions apply:

- The beam axis has a small initial deflection in the unloaded state, which is small compared to the length l
- The beam is slender, i.e. the height of the cross-section is small compared to the length l
- The layers are linearly elastic with arbitrary homogeneous cross-section whose parameters are constant over the length l
- The layers are rigid in shear and the cross-section remains constant
- The layers are elastically bonded in the longitudinal direction and rigidly bonded in the vertical direction
- The dynamic response is small compared to the height of the cross-section

Due to the flexible bond, the layers are translated longitudinally relative to each other at the layer boundaries under load, which is referred to as interlayer slip. A Cartesian coordinate system with the origin in the beam axis at the left support is used as the reference system. The x-coordinate describes the variation of the variables in the longitudinal direction of the member, the origin of the z-coordinate, which is directed vertically from top to bottom, is located in the beam axis and the y-coordinate is perpendicular to the $x-z$ plane. In the following, the equations of motion for a beam composed of three layers subjected to the vertical distributed time-varying load $p(x,t)$ are derived as an example as shown in Fig. 1. However, the derivation for a beam of two layers or for a beam with more than three layers can be carried out without additional assumptions and is thus straightforward. The top layer is indicated with the subscript $i=1$, the central layer with $i=2$ and the bottom layer with $i=3$. The beam axis is the line connecting the elastic centers of gravity of the composite cross-section, which therefore corresponds to the beam axis of the associated beam in which the layers are rigidly connected. The slight initial deflection in the stress-free state is referred to as $\hat{w}(x)$. Depending on the geometry of the cross-section and elastic stiffness, the beam axis can be located in any of the three layers. For the following representation of the longitudinal displacement field, it is however assumed that the beam axis is located in the second layer as depicted in Fig. 1. Nevertheless, the formulation of the displacement field for a different position of the beam axis can be done without additional effort.

Since the individual layers are supposed to be rigid in shear, the kinematic assumptions of Euler–Bernoulli theory can be applied to each layer separately. The deflection, which is superposed to the initial deflection $\hat{w}(x)$, is therefore, in addition to time t, only a function of x in each fiber of the three layers: $w_i(x,t)=w(x,t)$. The longitudinal displacement of a point in the ith layer at x and the distance ζ_i from the local center of gravity of this layer is composed of the longitudinal displacement $u_i^{(0)}(x,t)$ of this center of gravity and the contribution due to the cross-sectional rotation $w_{,x}(x,t)$,

$$u_i(x,\zeta_i,t)=u_i^{(0)}(x,t)-\zeta_i w_{,x}(x,t) \qquad i=1,2,3 \tag{1}$$

As shown in Fig. 2, the longitudinal displacements of the local center of gravity of the second and third layer $u_2^{(0)}(x,t)$ and $u_3^{(0)}(x,t)$ and the longitudinal displacement of the beam axis $u^{(\infty)}(x,t)$ can then be expressed as follows

$$u_2^{(0)}(x,t)=u_1^{(0)}(x,t)-\left(z_2-z_1\right)w_{,x}(x,t)+\Delta u_1(x,t) \tag{2}$$

$$u_3^{(0)}(x,t)=u_1^{(0)}(x,t)-\left(z_3-z_1\right)w_{,x}(x,t)+\Delta u_1(x,t)+\Delta u_2(x,t) \tag{3}$$

$$u^{(\infty)}(x,t)=u_1^{(0)}(x,t)+z_1 w_{,x}(x,t)+\Delta u_1(x,t) \tag{4}$$

as a function of $u_1^{(0)}(x,t)$, $w_{,x}(x,t)$ and the interlayer slip between the top and the central layer $\Delta u_1(x,t)$ and the interlayer slip between the central and the bottom layer $\Delta u_2(x,t)$. In the above equations z_1 (z_3) is the vertical coordinate from the beam axis to the centroid of the top (bottom) layer, see Fig. 1. By rearranging Eq. (4), $u_1^{(0)}(x,t)$ is written as a function of $u^{(\infty)}(x,t)$,

$$u_1^{(0)}(x,t)=u^{(\infty)}(x,t)-z_1 w_{,x}(x,t)-\Delta u_1(x,t) \tag{5}$$

Once the displacement field of the member is defined, the strains can be introduced. For linear small amplitude vibrations, the strain at the centroid of the ith layer is composed of the derivative of the horizontal displacement of the centroid $u_i^{(0)}(x,t)$ with respect to x and the contribution $w_{,x}(x,t)\hat{w}_{,x}(x)$ due to the initial deflection $\hat{w}(x)$,

$$e_i(x,t)=u_{i,x}^{(0)}(x,t)+w_{,x}(x,t)\hat{w}_{,x}(x), \qquad i=1,2,3 \tag{6}$$

For moderately large nonlinear vibrations of homogeneous slightly curved beams, the corresponding expression can be found in [43]. However, since in the present problem only small linear vibrations of slightly curved composite beams are analyzed, the nonlinear part of the longitudinal strain is dropped. The strain of any fiber in the ith layer becomes

$$\begin{aligned}\epsilon_i(x,\zeta_i,t)&=e_i(x,t)-\zeta_i w_{,xx}(x,t)\\&=u_{i,x}^{(0)}(x,t)+w_{,x}(x,t)\hat{w}_{,x}(x)-\zeta_i w_{,xx}(x,t), \qquad i=1,2,3\end{aligned} \tag{7}$$

Since the beam under consideration is stressed in the linear elastic range, Hooke's law is applicable. Accordingly, multiplying the longitudinal strains $\epsilon_i(x,\zeta_i)$ by the modulus of elasticity E_i of the ith layer leads to the longitudinal stresses in this layer. Layerwise integration of these stresses yields the axial forces in the individual layers,

$$N_i=EA_i e_i=EA_i\left(u_{i,x}^{(0)}+w_{,x}\hat{w}_{,x}\right), \qquad i=1,2,3 \tag{8}$$

which, after inserting relations Eqs. (2), (3) and (5), can be expressed by the applicable derivatives of the kinematic variables $w, u^{(\infty)}, \Delta u_1, \Delta u_2$ as follows,

$$N_1=EA_1 e_1\,, \quad e_1=\left(u_{,x}^{(\infty)}-z_1 w_{,xx}+w_{,x}\hat{w}_{,x}-\Delta u_{1,x}\right) \tag{9}$$

$$N_2=EA_2 e_2\,, \quad e_2=\left(u_{,x}^{(\infty)}-z_2 w_{,xx}+w_{,x}\hat{w}_{,x}\right) \tag{10}$$

$$N_3=EA_3 e_3\,, \quad e_3=\left(u_{,x}^{(\infty)}-z_3 w_{,xx}+w_{,x}\hat{w}_{,x}+\Delta u_{2,x}\right) \tag{11}$$

where $EA_i=E_iA_i$, $i=1,2,3$, is the axial stiffness and A_i the cross-sectional area of the ith layer. Integration of the longitudinal stresses multiplied by ζ_i over the ith cross-sectional area leads to the layerwise bending moments [44],

$$M_i=-EJ_i w_{,xx}, \qquad i=1,2,3 \tag{12}$$

with $EJ_i=E_iJ_i$ denoting the bending stiffness and J_i the area moment of inertia about the η_i-axis (see Fig. 1) of the ith layer. The overall axial

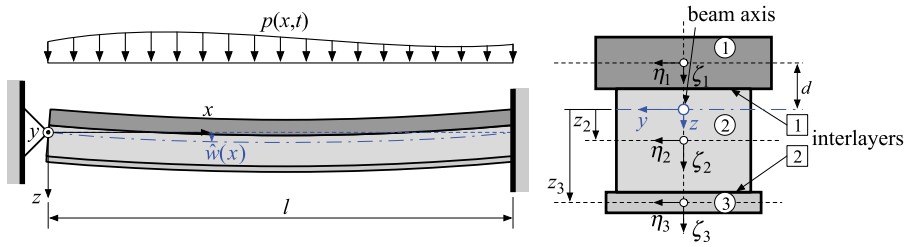

Fig. 1. Slightly curved beam composed of three elastically bonded layers.

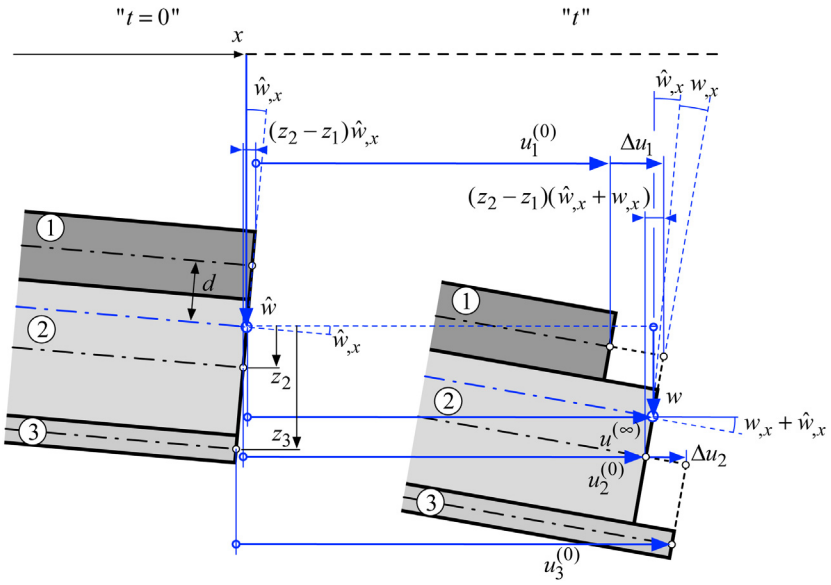

Fig. 2. Cross-section of a three-layer beam with interlayer slip at x in its initial (time $t = 0$) and its deformed state (time t).

force N and the overall bending moment M are related to the layerwise internal forces as

$$N = \sum_{i=1}^{3} N_i \tag{13}$$

$$M = \sum_{i=1}^{3} \left(M_i + N_i z_i \right) \tag{14}$$

The interlaminar shear traction $t_{s1}(x,t)$ between in the interface between the top and the central layer is proportional the interlayer slip $\Delta u_1(x,t)$, correspondingly, $t_{s2}(x,t)$ is proportional to $\Delta u_2(x,t)$,

$$t_{s1} = K_{s1} \Delta u_1 \,, \qquad t_{s2} = K_{s2} \Delta u_2 \tag{15}$$

where K_{s1} denotes the slip modulus in the upper interface and K_{s2} the slip modulus in the lower interface. The free-body diagram of an infinitesimal beam element in Fig. 3 shows the layerwise and overall internal forces.

3. Boundary value problem

3.1. Application of Hamilton's principle

After the basic relationships have been defined, the boundary value problem is derived. The most straightforward way to do this is to use Hamilton's principle, as this provides not only the equations of motion but also the boundary conditions. Here it should be noted that the dynamic response of the beam problem at hand is fully defined by the deflection w, the longitudinal displacement of the beam axis $u^{(\infty)}$ and the two interlayer slips Δu_1 and Δu_2.

According to Hamilton's principle for a conservative deformable system, the variation of the time integral over the Lagrangian $L = T - (U + W)$ is zero [45],

$$\int_{t_1}^{t_2} (\delta T - \delta U - \delta W) dt = 0 \tag{16}$$

where T denotes the kinetic energy, and U is the potential of the internal and W the potential of the external forces. Since the dynamic response of the considered structural member is studied in the lower frequency range, the longitudinal and rotational inertia are neglected. Only the inertia in the z-direction is considered, and thus the kinetic energy reads

$$T = \frac{1}{2} \int_0^l \mu \dot{w}^2(x,t) dx \tag{17}$$

with $\mu = \sum_{i=1}^{3} \rho_i A_i$ denoting the mass per unit length and ρ_i the mass density of the ith layer. The potential energy of the internal forces is expressed in terms of the layerwise bending moments M_i and axial forces N_i $(i = 1,2,3)$ and the shear tractions t_{s1} and t_{s2},

$$U = \frac{1}{2} \int_0^l \Big(\sum_{i=1}^{3} \big(M_i(x,t)(-w_{,xx}(x,t)) + N_i(x,t) e_i(x,t) \big) + \sum_{j=1}^{2} t_{sj}(x,t) \Delta u_j(x,t) \Big) dx \tag{18}$$

Since the external force $p(x,t)$ is applied in the z-direction only, the potential of the external forces is as follows

$$W = -\int_0^l p(x,t) w(x,t) dx \tag{19}$$

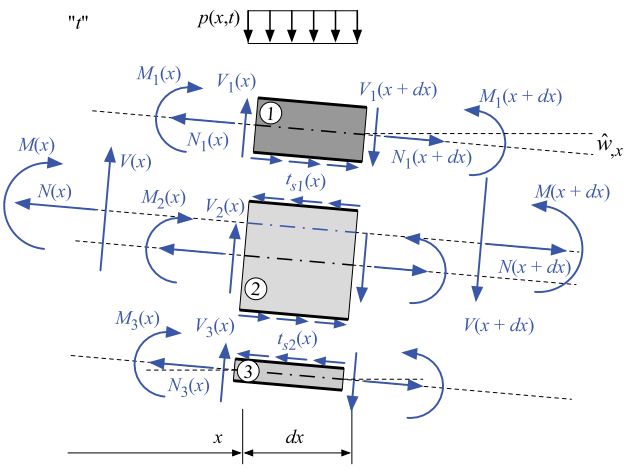

Fig. 3. Free-body diagram of an infinitesimal three-layer beam element at time t.

These expressions are inserted into Eq. (16), and application of the principles from the calculus of variations yields

$$\int_{t_1}^{t_2}\Bigg\{\int_0^l\Bigg(\sum_{i=1}^{3}(\mu\ddot{w}-M_{i,xx}-N_{i,xx}z_i-N_i\hat{w}_{,xx} - N_{i,x}\hat{w}_{,x}-p)\delta w+\sum_{i=1}^{3}(-N_{i,x})\delta u^{(\infty)} + (N_{1,x}+t_{s1})\delta\Delta u_1+(-N_{3,x}+t_{s2})\delta\Delta u_2\Bigg)dx + \Bigg[\sum_{i=1}^{3}(-M_i-N_iz_i)\delta w_{,x}+\sum_{i=1}^{3}(M_{i,x}+N_{i,x}z_i + N_i\hat{w}_{,x})\delta w+\sum_{i=1}^{3}N_i\delta u^{(\infty)} - N_1\delta\Delta u_1+N_3\delta\Delta u_2\Bigg]_0^l\Bigg\}dt=0 \tag{20}$$

According to the calculus of variations, the coefficients δw, $\delta u^{(\infty)}$, $\delta\Delta u_1$ and $\delta\Delta u_2$ are independent of each other. Therefore, the expressions in the brackets before these coefficients must vanish, and they correspond to the four equations of motion of the beam problem under consideration. In particular, combining all terms multiplied by δw and considering the relations Eqs. (13) and (14) leads to the first equation of motion,

$$\mu\ddot{w}-M_{,xx}-N\hat{w}_{,xx}=p \tag{21}$$

Note that in this respect $\sum_{i=1}^{3}N_{i,x}\hat{w}_{,x}=\hat{w}_{,x}\sum_{i=1}^{3}N_{i,x}=\hat{w}_{,x}N_{,x}=0$ because

$$N_{,x}=0 \tag{22}$$

which results from the vanishing terms multiplied by $\delta u^{(\infty)}$. The further equations of motion are related to $\delta\Delta u_1$ and $\delta\Delta u_2$ and read, compare with (20),

$$N_{1,x}+t_{s1}=0 \tag{23}$$

$$N_{3,x}-t_{s2}=0 \tag{24}$$

The boundary terms in Eq. (20) represent the pertaining classical boundary conditions of a slightly curved three-layer beam with interlayer slip without elastic constraints (springs) and lumped masses at the boundaries. Considering again the relations Eqs. (13) and (14), the five boundary conditions are identified as follows,

$$(w_{,x})_b=0 \quad\text{or}\quad M_b=0, \qquad w_b=0 \quad\text{or}\quad (M_{,x})_b+N_b(\hat{w}_{,x})_b=0,$$
$$u_b^{(\infty)}=0 \quad\text{or}\quad N_b=0,$$
$$(\Delta u_1)_b=0 \quad\text{or}\quad (N_1)_b=0, \qquad (\Delta u_2)_b=0 \quad\text{or}\quad (N_3)_b=0 \tag{25}$$

where the subscript b indicates a boundary (i.e. $x=0$ or $x=l$).

It should be noted that the same set of equations of motion Eqs. (21)–(24) would be obtained by application of conservation of momentum and conservation of angular momentum to the forces of the free-body diagram of an infinitesimal beam element shown in Fig. 3 but with the disadvantage that such an approach does not provide the boundary conditions.

3.2. Equations of motion expressed by the governing kinematic variables

For the solution of this boundary value problem, it is advantageous to express the equations of motion by the governing kinematic variables w, $u^{(\infty)}$, Δu_1, Δu_2 and their derivatives with respect to x and t. First, the overall bending moment M is written as a function of the kinematic variables, since this internal force enters the first equation of motion Eq. (21). Substituting Eqs. (9)–(12) into Eq. (14) leads to

$$M=-EJ_\infty w_{,xx}-EA_1z_1\Delta u_{1,x}+EA_3z_3\Delta u_{2,x} \tag{26}$$

where EJ_∞ is the bending stiffness of the member whose layers are rigidly bonded, and EJ_0 is the bending stiffness of the beam whose layers are not bonded,

$$EJ_\infty=EJ_0+\sum_{i=1}^{3}EA_iz_i^2\,, \quad EJ_0=\sum_{i=1}^{3}EJ_i \tag{27}$$

The first equation of motion is then obtained by substituting Eq. (26) into Eq. (21),

$$\mu\ddot{w}+EJ_\infty w_{,xxxx}+EA_1z_1\Delta u_{1,xxx}-EA_3z_3\Delta u_{2,xxx}-N\hat{w}_{,xx}=p \tag{28}$$

Next, Eqs. (9) through (11) are substituted into Eq. (13), yielding the overall axial force

$$N=EA_e\left(u_{,x}^{(\infty)}+w_{,x}\hat{w}_{,x}\right)-EA_1\Delta u_{1,x}+EA_3\Delta u_{2,x} \tag{29}$$

which is subsequently inserted into Eq. (22) to obtain the second equation of motion,

$$EA_e\left(u_{,xx}^{(\infty)}+w_{,x}\hat{w}_{,xx}+w_{,xx}\hat{w}_{,x}\right)-EA_1\Delta u_{1,xx}+EA_3\Delta u_{2,xx}=0\,,$$
$$EA_e=\sum_{i=1}^{3}EA_i \tag{30}$$

Since according to Eq. (22) the overall axial force is constant along the span, it is convenient to use the following integral representation for

N when analyzing the vibration response,

$$N = \frac{EA_e}{l}\int_0^l \left(u_{,x}^{(\infty)} + w_{,x}\hat{w}_{,x}\right)dx - \frac{EA_1}{l}\int_0^l \Delta u_{1,x}dx + \frac{EA_3}{l}\int_0^l \Delta u_{2,x}dx \tag{31}$$

as used, for example, in [43] for the analysis of dynamic buckling of homogeneous slightly curved beams.

Finally, substituting Eqs. (9), (11) and (15) into Eqs. (23) and (24) delivers the third and fourth equation of motion,

$$EA_1\left(u_{,xx}^{(\infty)} - z_1 w_{,xxx} + w_{,x}\hat{w}_{,xx} + w_{,xx}\hat{w}_{,x} - \Delta u_{1,xx}\right) + K_{s1}\Delta u_1 = 0\,, \tag{32}$$

$$EA_3\left(u_{,xx}^{(\infty)} - z_3 w_{,xxx} + w_{,x}\hat{w}_{,xx} + w_{,xx}\hat{w}_{,x} + \Delta u_{2,xx}\right) - K_{s2}\Delta u_2 = 0 \tag{33}$$

3.3. Classical boundary conditions expressed by the governing kinematic variables

The boundary conditions Eq. (25) are specified for a hinged end without shear restraints (acronym S), a hard-hinged end (H), a clamped (C) and a free end (F). In addition, the beam can be horizontally immovable (I) or movable (M).

Hinged support without shear restraints (soft-hinged support, S). At a hinged support without shear restraints, referred to as soft-hinged support, the deflection is zero,

$$w_b^{(\infty)} = 0 \tag{34}$$

Moreover, the overall moment and the normal forces in the top and the bottom layer are zero,

$$M_b^{(\infty)} = 0\,,\quad (N_1)_b = 0\,,\quad (N_3)_b = 0 \tag{35}$$

Expressed in terms of the kinematic variables according to Eqs. (26), (9) and (11), the latter boundary conditions read

$$-EJ_\infty (w_{,xx})_b - EA_1 z_1 (\Delta u_{1,x})_b + EA_3 z_3 (\Delta u_{2,x})_b = 0 \tag{36}$$

$$(u_{,x}^{(\infty)})_b - z_1 (w_{,xx})_b + (w_{,x})_b(\hat{w}_{,x})_b - (\Delta u_{1,x})_b = 0 \tag{37}$$

$$(u_{,x}^{(\infty)})_b - z_3 (w_{,xx})_b + (w_{,x})_b(\hat{w}_{,x})_b + (\Delta u_{2,x})_b = 0 \tag{38}$$

If the support is horizontally immovable, then

$$u_b^{(\infty)} = 0 \qquad \text{(horizontally immovable, I)} \tag{39}$$

and the overall axial force is transferred to the second layer, i.e. $(N_2)_b = N_b$. In the case of a horizontally sliding support, on the other hand, the overall normal force is zero at the boundary,

$$N_b = 0 \qquad \text{(horizontally moveable, M)} \tag{40}$$

expressed in terms of the kinematic variables, Eq. (29),

$$EA_e\left((u_{,x}^{(\infty)})_b + (w_{,x})_b(\hat{w}_{,x})_b\right) - EA_1(\Delta u_{1,x})_b + EA_3(\Delta u_{2,x})_b = 0 \qquad \text{(horizontally sliding)} \tag{41}$$

Hard-hinged support (H). In a hard-hinged support, a rigid plate at the end cross-section restrains the relative displacement between the layers at the edge, i.e.

$$(\Delta u_1)_b = (\Delta u_2)_b = 0 \tag{42}$$

The deflection and the overall bending moment are zero, i.e. the boundary conditions Eqs. (34) and (36) apply. Depending on whether the boundary is horizontally sliding or horizontally restrained, the boundary condition Eq. (39) or Eq. (41) applies.

Rigidly clamped end (CI). No movement is possible at a rigidly clamped end, thus in addition to zero deflection (Eq. (34)), zero horizontal displacement (Eq. (39)) and zero interlayer slips (Eq. (42)), also the cross-sectional rotation is zero,

$$(w_{,x})_b = 0 \tag{43}$$

Free end (F). At a free end, all dynamic boundary conditions are zero, i.e.

$$M_b = 0,\quad (M_{,x})_b = 0,\quad (N_1)_b = 0,\quad (N_3)_b = 0,\quad N_b = 0\ \ ((N_2)_b = 0) \tag{44}$$

see Eq. (25), or expressed by the kinematic variables, the boundary conditions according to Eqs. (36), (37), (38), (41) hold and it follows from $(M_{,x})_b + N_b(\hat{w}_{,x})_b = 0$, see Eq. (26),

$$-EJ_\infty (w_{,xxx})_b - EA_1 z_1 (\Delta u_{1,xx})_b + EA_3 z_3 (\Delta u_{2,xx})_b + N_b(\hat{w}_{,x})_b = 0 \tag{45}$$

As can be seen from these equations, the analytical solution of the boundary value problem is most challenging when one end is soft-hinged supported without shear restraints and both ends are horizontally restrained, since in this case all kinematic variables are coupled via the boundary conditions.

The complete set of equations of motion and corresponding boundary conditions, which captures the linear dynamic response of slightly curved composite beams with interlayer slip, can be solved exactly for simple cases or is the starting point for approximate solutions.

4. Vibration analysis

In the following, the proposed theory is used to analyze the vibration response of two different beam configurations. In the first case, the beams are composed of three symmetrically arranged layers. In one study, both beam ends are soft-hinged supported and completely immovable; in another study, one support of the beam is horizontally sliding. For these boundary value problems, an analytical solution of the dynamic response is found. In contrast, the second problem, which involves flexibly bonded two-layer beams, is solved numerically.

4.1. Soft-hinged immovably supported three-layer beam with symmetric layer arrangement (SI-SI)

The symmetrical layer structure simplifies the boundary value problem considerably. The bending stiffness and longitudinal stiffness of the top and the bottom layer are equal, and also the slip modulus of both interfaces are the same. Thus, in Eqs. (32)–(28)

$$EJ_3 = EJ_1,\quad EA_3 = EA_1,\quad K_{s2} = K_{s1},\quad z_3 = -z_1 = d \tag{46}$$

and the beam axis coincides with the axis of the central layer, i.e. $u^{(\infty)} = u_2^{(0)}$. The member is soft-hinged supported, i.e. Eqs. (34), (36)–(38) apply. Moreover, it is assumed that both ends are horizontally restrained, thus additionally to boundary condition Eq. (34) boundary condition Eq. (39) applies. The most significant simplifications resulting from the symmetric layer arrangement, however concern the remaining three dynamic boundary conditions. Subtracting Eq. (38) from Eq. (37) and substituting the outcome into Eq. (36), reveals that

$$(w_{,xx})_b = 0 \tag{47}$$

$$(\Delta u_{1,x})_b + (\Delta u_{2,x})_b = 0 \tag{48}$$

i.e., the curvature $(w_{,xx})_b$ is decoupled from the slope of the interlayer slips $(\Delta u_{1,x})_b$ and $(\Delta u_{2,x})_b$. The summation of Eqs. (38) and (37) gives the fifth boundary condition in a form that is favorable for solving this boundary value problem,

$$2\left(u_{,x}^{(\infty)} + w_{,x}\hat{w}_{,x}\right)_b + (\Delta u_{2,x} - \Delta u_{1,x})_b = 0 \tag{49}$$

Note that this equation is equivalent of the overall normal force being transferred to the central layer at the support, i.e. $(N_2)_b = (N)_b$.

Furthermore, the small initial deflection is supposed to have the form of a sine half-wave or a multiple thereof

$$\hat{w}(x) = \hat{w}_0 \sin(\lambda_k x)\,,\qquad \lambda_k = \frac{k\pi}{l}\,,\qquad k \in \mathbb{N}^+ \tag{50}$$

with $\hat{w}_0$ denoting the amplitude of the initial deflection.

Free vibration analysis. As shown in previous studies (e.g. [11,46]), the eigenfunctions for the deflection of a soft-hinged supported single-span beam with interlayer slip and straight member axis correspond to a sine half-wave or a multiple thereof,

$$W^{(i)}(x) = \gamma_i \sin(\lambda_i x) \ , \quad \lambda_i = \frac{i\pi}{l} \ , \quad i = 1,2,3,\dots \tag{51}$$

with γ_i denoting an arbitrary scaling coefficient of the ith mode. Since the same boundary conditions apply as for the straight beam (i.e. $w_b = (w_{,xx})_b = 0$), and the initial deflection is proportional to at least one of the eigenfunctions of the straight beam, the eigenfunctions of the symmetrically layered soft-hinged supported beam are identical to those of the corresponding straight beam with interlayer slip.

Before the natural angular frequencies can be calculated, the eigenfunctions $\Delta U_1^{(i)}, \Delta U_2^{(i)}$ for the interlayer slips $\Delta u_1, \Delta u_2$ and $U^{(\infty)(i)}$ for the longitudinal displacement of the beam axis $u^{(\infty)}$ are determined. To this end, the ith eigenfunction for the deflection Eq. (51) and the initial deflection in the form of a sinusoidal function Eq. (50) are substituted into the equations of motion Eqs. (30), (32) and (33) instead of the corresponding kinematic variables. This set of equations is solved analytically together with the boundary conditions Eqs. (39), (48) and (49) with the result

$$\Delta U_1^{(i)}(x) = \gamma_i \lambda_i^2 \left(\frac{d\,\lambda_i \cos(\lambda_i x)}{\lambda_i^2 + \frac{K_{s1}}{EA_1}} - \frac{1}{2}\beta(x)\hat{w}_0\delta_{ik} \right) \ , \quad i = 1,2,3,\dots \tag{52}$$

$$\Delta U_2^{(i)}(x) = \gamma_i \lambda_i^2 \left(\frac{d\,\lambda_i \cos(\lambda_i x)}{\lambda_i^2 + \frac{K_{s1}}{EA_1}} + \frac{1}{2}\beta(x)\hat{w}_0\delta_{ik} \right) \ , \quad i = 1,2,3,\dots \tag{53}$$

$$U^{(\infty)(i)}(x) = \gamma_i \frac{\lambda_i \hat{w}_0 k}{(k-i)(k+i)} \left(i\cos(\lambda_k x)\sin(\lambda_i x) - k\cos(\lambda_i x)\sin(\lambda_k x) \right), \quad i \neq k \tag{54}$$

$$U^{(\infty)(i)}(x) = \gamma_k \lambda_k^2 \hat{w}_0 \frac{1}{2} \left(-\frac{1}{\lambda_{2k}} \sin(\lambda_{2k} x) + \theta(x) \right) \ , \quad i = k \tag{55}$$

where

$$\begin{aligned} \beta(x) &= \frac{EA_e l \sinh\left(\frac{1}{2}\kappa(l-2x)\right)}{4EA_1 \sinh\left(\frac{\kappa l}{2}\right) + EA_2 \kappa l \cosh\left(\frac{\kappa l}{2}\right)} \ , \\ \theta(x) &= \frac{2EA_1 \left((l-2x)\sinh\left(\frac{\kappa l}{2}\right) - l \sinh\left(\frac{1}{2}\kappa(l-2x)\right) \right)}{4EA_1 \sinh\left(\frac{\kappa l}{2}\right) + EA_2 \kappa l \cosh\left(\frac{\kappa l}{2}\right)} \end{aligned} \tag{56}$$

$$\kappa = \left(\frac{EA_e K_{s1}}{EA_1 EA_2} \right)^{1/2} \tag{57}$$

δ_{ik} denotes the Kronecker delta. Eqs. (52) and (53) show that the initial deflection only affects the kth eigenfunction for the interlayer slip, i.e. $\Delta U_1^{(k)}$ and $\Delta U_2^{(k)}$ are different, while the remaining eigenfunctions are the same, i.e. $\Delta U_1^{(i)} = \Delta U_2^{(i)}, i \neq k$. Substituting the eigenfunctions Eqs. (51) to (55) into the boundary conditions Eqs. (34), (39), (47), (48) and (49) shows that they are satisfied, which also confirms that the eigenfunctions of the deflection correspond to those of the straight member.

Eventually, evaluation of Eq. (31) with the eigenfunctions of the kinematic variables leads to the following modal expression of the overall normal force N,

$$N_{ef}^{(i)} = \frac{\psi}{2} \gamma_k \hat{w}_0 \lambda_k^2 \delta_{ik} \ , \quad i = 1,2,3,\dots \tag{58}$$

where

$$\psi = \frac{EA_e EA_2 \kappa l \cosh\left(\frac{\kappa l}{2}\right)}{4EA_1 \sinh\left(\frac{\kappa l}{2}\right) + EA_2 \kappa l \cosh\left(\frac{\kappa l}{2}\right)} \tag{59}$$

Accordingly, only the kth modal overall normal force is non-zero, indicating that the initial deflection $\hat{w}$ induces this internal force.

To determine the natural angular frequencies ω_i, $i = 1,2,3,\dots$, the kinematic variables and the normal force are assumed as

$$\begin{aligned} &w(x,t) = W^{(i)}(x)\sin\omega_i t \ , \quad \Delta u_1(x,t) = \Delta U_1^{(i)}(x)\sin\omega_i t \ , \\ &\Delta u_2(x,t) = \Delta U_2^{(i)}(x)\sin\omega_i t \ , \\ &N(t) = N_{ef}^{(i)} \sin\omega_i t \end{aligned} \tag{60}$$

and inserted into the homogeneous form of the fourth equation of motion Eq. (28) (i.e. $p(x,t) = 0$). This finally leads to

$$\omega_i = \left(\frac{1}{\mu}\lambda_i^4 \left(\lambda_i^2 + \alpha^2\right) \left(\frac{\alpha^2}{EJ_\infty} + \frac{\lambda_i^2}{EJ_0} \right)^{-1} + \frac{1}{2\mu}\psi\lambda_k^4 \hat{w}_0^2 \delta_{ik} \right)^{1/2} \ , \quad i = 1,2,3,\dots \tag{61}$$

where

$$\alpha = \left(\frac{EJ_\infty K_{s1}}{EA_1 EJ_0} \right)^{1/2} \tag{62}$$

This equation shows that only the kth natural angular frequency, whose corresponding eigenfunction is proportional to the initial deflection, is affected by the initial deflection.

Forced vibration analysis. Once the natural frequencies and the eigenfunctions are known, modal analysis (e.g. [47]) is applied to determine the forced beam vibrations. To this end, the deflection, the two interlayer slips and the normal force are modally expanded,

$$\begin{aligned} &w(x,t) = \sum_{i=1}^{\infty} W^{(i)}(x) Y_i(t) \ , \quad \Delta u_1(x,t) = \sum_{i=1}^{\infty} \Delta U_1^{(i)}(x) Y_i(t) \ , \\ &\Delta u_2(x,t) = \sum_{i=1}^{\infty} \Delta U_2^{(i)}(x) Y_i(t) \ , \\ &u^{(\infty)}(x,t) = \sum_{i=1}^{\infty} U^{(\infty)(i)} Y_i(t) \ , \quad N(t) = N_{ef}^{(k)} Y_k(t) \end{aligned} \tag{63}$$

These modal series are inserted into the equation of motion Eq. (28), which is multiplied by the jth eigenfunction W_j. Integration of this expression over the beam length l and choosing the scale factor for the eigenfunctions of one, i.e. $\gamma_i = 1$, $i = 1,2,3,\dots$, provides the modal equations for the modal coordinates Y_i,

$$\ddot{Y}_i + \omega_i^2 Y_i = \frac{2}{\mu l} p_i \ , \quad i = 1,2,3,\dots \tag{64}$$

with the modal load

$$p_i(t) = \int_0^l W^{(i)}(x) p(x,t) dx \ , \quad i = 1,2,3,\dots \tag{65}$$

By adding modal damping in analogy to the single-degree-of freedom oscillator, characterized by the modal damping coefficient ζ_i, $i = 1,2,3,\dots$, the effect of the damping is also taken into account in a simple manner (e.g. [47]),

$$\ddot{Y}_i + 2\zeta_i \omega_i \dot{Y}_i + \omega_i^2 Y_i = \frac{2}{\mu l} p_i \ , \quad i = 1,2,3,\dots \tag{66}$$

The solution of these equations is obtained by standard methods of linear vibration theory. Substituting the modal coordinates Y_i, $i = 1,2,3,\dots$, back into the modal series Eq. (63), which are approximated by a finite number of modes, yields the vibration response of the beam under consideration.

4.2. Three-layer beam with symmetric layer arrangement with one horizontally sliding support

Again, a symmetrically layered beam with interlayer slip is considered as defined in Eq. (46), but the support at the right boundary $x = l$ is horizontally sliding (M), i.e. $u^{(\infty)}(x = l) \neq 0$. Apart from that, the

supports can be soft-hinged (S), hard-hinged (H), clamped (C), or free (F).

According to Eq. (25), $u^{(\infty)}(x=l)\neq 0$ implies that at this boundary the axial force is zero, $N(x=l)=0$. Consequently, the axial force along the entire span is zero, $N(x)=0$, $0\le x\le l$, since $N_{,x}(x)=0$ (Eq. (22)). This, together with the symmetrical layer arrangement, results in $\Delta u_1(x)=\Delta u_2(x)$, and the boundary value problem is simplified considerably. Thus, Eq. (28) becomes

$$\mu\ddot{w}+EJ_\infty w_{,xxxx}-2EA_1 d\,\Delta u_{1,xxx}=p \tag{67}$$

Furthermore, it follows from Eq. (29) that

$$u^{(\infty)}_{,x}+w_{,x}\hat{w}_{,x}=0 \tag{68}$$

Therefore, the two equations of motion Eqs. (32) and (33) reduce to a single equation,

$$EA_1\left(d\,w_{,xxx}-\Delta u_{1,xx}\right)+K_{s1}\Delta u_1=0 \tag{69}$$

Eqs. (67) and (69) correspond to the equations of motion of the straight three-layer beam with symmetrically arranged layers and interlayer slip known from the literature. Hence, the deflection and the interlayer slip of the slightly curved beam are equal to those of the corresponding beam with straight beam axis since the boundary conditions defined in Section 3.3 also simplify to those of the straight beam, for instance for a soft-hinged support (S)

$$w_b=0\ ,\quad (w_{,xx})_b=0\ ,\quad (\Delta u_{1,x})_b=0 \tag{70}$$

The solution of equations of motion Eqs. (67) and (69) for the straight beam with interlayer slip along with the boundary conditions has been know for a long time, and reference is therefore made to the relevant literature (e.g. [11,12,14,15]). However, it should only be noted here that these two equations and the corresponding boundary conditions can be decoupled from each other for simpler solving and expressed by one equation only in w and a second equation only in Δu_1 (see e.g. [15]). For instance, for the deflection w a partial differential equation of sixth order results.

However, unlike the straight beam, the longitudinal displacement of the central axis $u^{(\infty)}$ is non-zero and results from Eq. (68) with the boundary condition $u^{(\infty)}(x=0)=0$ after w has been computed.

Free and forced vibration analysis of a soft-hinged beam (SI-SM). As an example, consider a symmetrically laminated beam with interlayer slip, soft-hinged supported at both ends (SI-SM) and slightly curved in the form of a sine half-wave or a multiple of it, see Eq. (50). As discussed above, the deflection $w(x,t)$ corresponds to that of the beam with straight beam axis and thus the natural angular frequencies ω_i are those of the straight beam [1,12],

$$\omega_i=\left(\frac{1}{\mu}\lambda_i^4\left(\lambda_i^2+\alpha^2\right)\left(\frac{\alpha^2}{EJ_\infty}+\frac{\lambda_i^2}{EJ_0}\right)^{-1}\right)^{1/2}\ ,\quad i=1,2,3,\dots \tag{71}$$

and the eigenfunctions $W^{(i)}(x)$ for the deflection given in Eq. (51). Eq. (69) represents not only the relation between w and Δu_1 but also the relation between the ith eigenfunction $W^{(i)}$ for the deflection and the ith eigenfunction $\Delta U_1^{(i)}(x)$ for the interlayer slip. Therefore, $W^{(i)}(x)$ (Eq. (51)) is substituted into Eq. (69), which is then solved together with the boundary conditions $\Delta U^{(i)}_{1,x}(x=0)=\Delta U^{(i)}_{1,x}(x=l)=0$ for $\Delta U_1^{(i)}(x)$,

$$\Delta U_1^{(i)}(x)=\Delta U_2^{(i)}(x)=\gamma_i\frac{d\,\lambda_i^3\cos\left(\lambda_i x\right)}{\lambda_i^2+\frac{K_{s1}}{EA_1}}\ ,\quad i=1,2,3,\dots \tag{72}$$

The eigenfunctions $U^{(\infty)(i)}(x)$ for the longitudinal displacement of the central axis are obtained from Eq. (68), into which the $W^{(i)}(x)$ (Eq. (51)) and $\hat{w}(x)$ (Eq. (50)) are inserted, together with the boundary condition $U^{(\infty)(i)}(x=0)=0$. For the ith mode, whose deflection eigenfunction is proportional to the kth member of the initial deflection, the result is

$$U^{(\infty)(k)}(x)=\gamma_k\lambda_k^2\hat{w}_0\frac{1}{2}\left(-\frac{1}{\lambda_{2k}}\sin\left(\lambda_{2k}x\right)-x\right)\ ,\quad i=k \tag{73}$$

For the modes $i\neq k$ the same expression (Eq. (54)) is found as for the horizontally immovably supported beam.

Once the modal parameters are known, $w(x,t)$ and $\Delta u_1(x,t)$ are modally expanded according to Eq. (63). The subsequent application of modal analysis to Eq. (67) leads to the decoupled modal equations Eq. (64) or with added damping Eq. (66). The modal coordinates Y_i obtained from these equations are substituted into the modal expansion of $w(x,t)$, $\Delta u_1(x,t)$ and $u^{(\infty)}(x,t)$ approximated by a finite number of modes.

4.3. Three-layer beam example problems

In the first example, the natural frequencies and eigenfunctions of a symmetrically layered slightly curved beam with rectangular cross-section are computed, which has the following dimensions: layer thicknesses $h_1=h_3=0.01$ m, $h_2=0.0102$ m; layer width $b=0.1$ m; span width of $l=1.0$ m. The material properties are characterized by the following parameters: Young's modulus of the face layers $E_1=E_3=7.0\cdot10^{10}$ N/m^2; Young's modulus of the core layer $E_2=1.0\cdot10^{10}$ N/m^2; slip modulus $K_{s1}=1.0\cdot10^9$ N/m^2; density of the face layers $\rho_1=\rho_3=2700$ kg/m^3; density of the core layer $\rho_2=1000$ kg/m^3. The product of the layer interaction parameter α (Eq. (62)) and the length l is $\alpha l=13.3$, which corresponds to a moderate interaction of the layers [2]. The damping is set to zero to ensure comparability with the FE solution. Two cases of the soft-hinged supported beam are considered. In the first case, both supports are horizontally immovable (SI-SI), in the second case the support at $x=l$ is horizontally sliding (SI-SM).

The outcomes of the proposed beam theory are set in contrast to the results of a more elaborate finite element (FE) model assuming plane stress elasticity. This comparative model, whose solution is found with the software package Abaqus v. 2016 [48], does not require the Euler–Bernoulli hypothesis and is therefore more accurate than the beam theory, but is numerically much more expensive. In the FE model, the three layers are discretized with quadrilateral plane elements with eight nodes. A Poisson's ratio of 0.3 is assumed for the material of the layers. Between the layers, two very thin cohesive zones with a thickness of 0.1 mm, (i.e. $h_1/100$) are provided to simulate the flexible layer interaction. These zones are discretized with linear cohesive elements with four nodes per element. The tangential stiffness of these elements corresponds to the slip modulus K_{s1}, for the normal stiffness a very large value of $10,000K_{s1}$ is applied, as this quantity is infinite in the beam model. The height of the middle layer is reduced by the thickness of the cohesive zones (i.e. $h_2=0.01$ m) so that the total height of the beam remains the same. In the FE model a kinematic coupling of the outer surfaces of the middle layer at an additional node describe the soft-hinged supports. The FE model has about 40,000 degrees of freedom, compared to the $J=11$ degrees of freedom of the beam model (i.e. number of eigenfunctions included in the analysis).

First, the natural frequencies of the immovably soft-hinged supported beam (SI-SI) are considered, whose initial deflection in the form of a sine half-wave $\hat{w}(x)=\hat{w}_0\sin(\pi x/l)$ is proportional to the first deflection eigenfunction of the straight beam. Fig. 4(a) shows the first five natural frequencies ω_i, $i=1,\dots,5$, as a function of the amplitude of the initial deflection $\hat{w}_0$ normalized with the beam length l in the range $0\le|\hat{w}_0/l|\le0.08$. The natural frequencies ω_i are divided by the fundamental frequency of the straight beam $\omega_1(\hat{w}_0/l=0)=383.7$ rad/s. Since the beam is symmetrically layered, the natural frequencies apply to both negative and positive initial deflection $\pm\hat{w}_0/l$. The normalized natural frequencies as a result of the presented beam theory are shown with continuous lines. As observed and discussed earlier, only the natural frequency whose deflection eigenfunction is

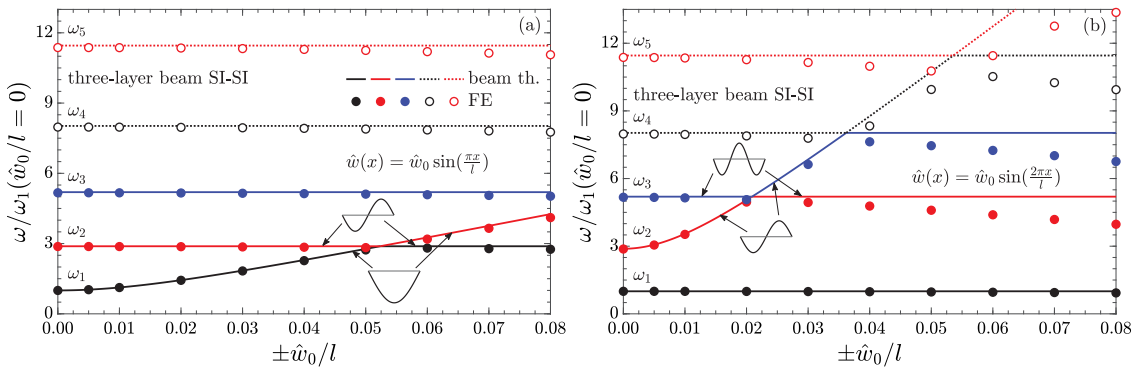

Fig. 4. First five natural frequencies as a function of the normalized amplitude of the initial deflection. Initial deflection (a) sine half-wave, (b) sine wave. Three-layer beam. Soft-hinged horizontally immovably supported.

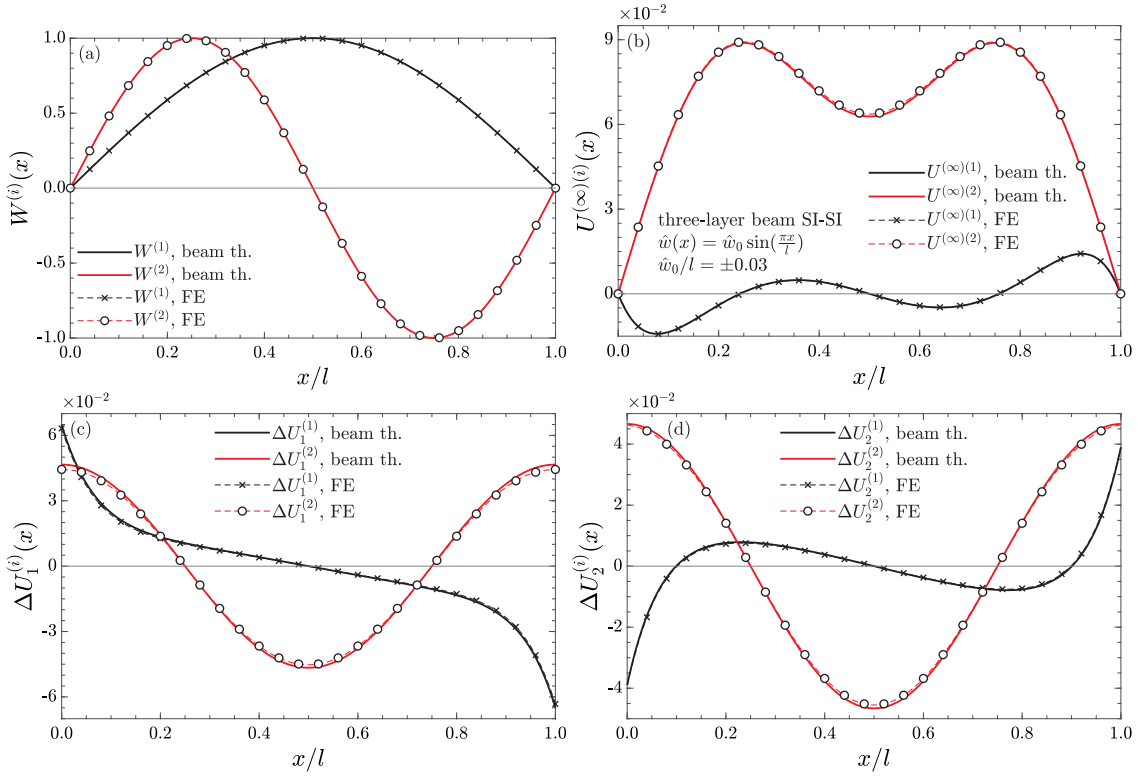

Fig. 5. First and second eigenfunction of the (a) deflection, (b) longitudinal displacement of the central axis, (c) upper interlayer slip, (d) lower interlayer slip. Initial deflection: sine half-wave. Three-layer beam. Soft-hinged horizontally immovably supported.

proportional to the initial deflection is affected by the initial deflection. This natural frequency increases with increasing $\hat{w}_0$ and corresponds to the fundamental frequency up to a ratio $|\hat{w}_0/l| = 0.0524$, and to the second natural frequency for $|\hat{w}_0/l| > 0.0524$. That is, for $|\hat{w}_0/l| > 0.0524$, the fundamental eigenfunction is a sine wave and the second eigenfunction is a sine half-wave. For discrete values of the amplitude of the initial deflection, these natural frequencies were also determined numerically by plane stress FE analyses, which are shown as markers in this figure. The comparison shows that in the whole studied range of $\hat{w}_0/l$, the considered natural frequencies of beam theory and plane stress theory agree very well. While for very small amplitudes $\hat{w}_0/l$ of the initial deflection up to 1% of the beam length both solutions are practically identical, the deviation of the beam theory solution increases slightly with increasing $\hat{w}_0/l$. For the largest considered initial deflection of $\hat{w}_0/l = \pm 0.08$, the fifth natural frequency ω_5 of the beam theory is 3.53% larger than that of the plane stress FE analysis.

For the case $\hat{w}_0/l = \pm 0.03$, Fig. 5 shows the first two eigenfunctions for the deflection $W^{(1)}$ and $W^{(2)}$ (Fig. 5(a)), the longitudinal displacement of the central axis $U^{(\infty)(1)}$ and $U^{(\infty)(2)}$ (Fig. 5(b)), the upper interlayer slip $\Delta U_1^{(1)}$ and $\Delta U_1^{(2)}$ (Fig. 5(c)), and the lower interlayer slip $\Delta U_2^{(1)}$ and $\Delta U_2^{(2)}$ (Fig. 5(d)) as a result of the beam theory (solid lines) and the plane stress FE analyses (dashed lines). As can be seen, the eigenfunctions of the two theories are virtually congruent, which confirms the proposed beam theory. The results also visualize that the initial deflection has no influence on the eigenfunction of the deflection (Fig. 5(a)), but on the shape of the first eigenfunction of the interlayer slips $\Delta U_1^{(1)}$ and $\Delta U_2^{(1)}$ (Fig. 5(c) and (d)). The comparison of Fig. 5(c) and (d) shows that $\Delta U_1^{(1)}$ and $\Delta U_2^{(1)}$ are different, while for the second mode $\Delta U_1^{(2)}$ and $\Delta U_2^{(2)}$ are identical and the same as for the straight beam.

In addition, the first two eigenfunctions for the interlayer slips and the longitudinal displacement are shown in Fig. 6 for this beam with the same initial deflection, but which is now *horizontally sliding at the*

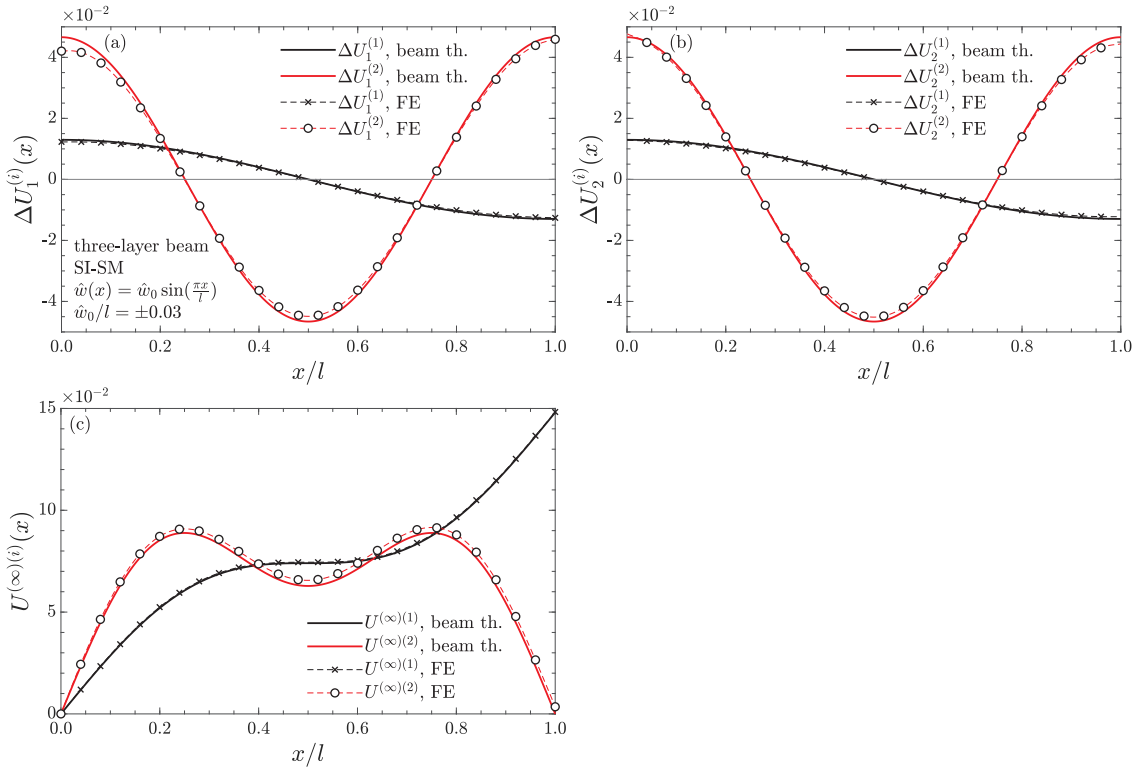

Fig. 6. First and second eigenfunction of the (a) upper interlayer slip, (b) lower interlayer slip, (c) longitudinal displacement of the central axis. Initial deflection: sine half-wave. Three-layer beam. Soft-hinged supported, right support horizontally sliding.

right support (SI-SM). In this case, the initial deflection has no influence on the eigenfunctions of the interlayer slips $\Delta U_1^{(i)}$, $\Delta U_2^{(1)}$ and, as in the case of the straight beam, they are identical for the upper and lower interlayer slips, $\Delta U_1^{(i)} = \Delta U_2^{(i)}$ (Fig. 6(a) and (b)). In contrast to the straight beam, however, the eigenfunctions $U^{(\infty)(1)}$ and $U^{(\infty)(2)}$ shown in Fig. 6(c) are non-zero. The natural frequencies as well as the eigenfunctions of the deflection correspond to those of the straight beam and are therefore not shown. Fig. 6 also demonstrates that the beam theory and the plane stress FE analysis provide virtually the same eigenfunctions for these boundary conditions as well.

In the second example, the initial deflection of the immovably soft-hinged supported beam (SI-SI) is proportional to the deflection eigenfunction of the second mode of the straight beam ($k = 2$ in Eqs. (50), (52)–(55)): $\hat{w}(x) = \hat{w}_0 \sin(2\pi x/l)$. As Fig. 4(b) shows, only the natural frequency of this mode increases with increasing $\hat{w}_0/l$, while the other eigenfunctions correspond to those of the straight beam. For this initial deflection in the form of a sine wave, up to $\hat{w}_0/l \approx \pm 0.03$, the considered natural frequencies of the beam theory agree very well with those of the FE plane stress outcomes. For the fundamental frequency this agreement is given for the whole considered range of $0 \leq |\hat{w}_0/l| \leq 0.08$, while for the higher modes the difference increases with increasing $\hat{w}_0/l$. The reason for this is the much stronger curvature at the same amplitude $\hat{w}_0/l$ compared to the sine half-wave of the first example, which cannot be considered as a small initial curvature (i.e., it is deep curvature). At $\hat{w}_0/l = \pm 0.08$ the second natural frequency based on the beam theory is already 30.8% larger than that of the FE plane stress prediction. Also for this beam with an initial deflection in the form of a sine wave, the first two eigenfunctions for the kinematic variables are shown in Fig. 7 as an example for the amplitude of initial deflection $\hat{w}_0/l = \pm 0.03$. Again, the results of the beam theory agree very well with the outcomes of the plane stress FE analyses.

As a third example, the forced vibrations of the immovably soft-hinged supported beam (SI-SI) with an initial deflection according to a sine half-wave $\hat{w}(x) = \hat{w}_0 \sin(\pi x/l)$ with $\hat{w}_0/l = -0.01$ are considered. The time-harmonic load $p(x,t) = p_0\,(H(x) - H(x - l/2))\sin(\nu t)$, which is equally distributed over the left half of the beam, is applied at time $t = 0$; $H(.)$ denotes the Heaviside function. The excitation frequency ν is 1.3 times the first natural frequency of the slightly curved beam, i.e. $\nu/\omega_1 = 1.3$. For the beam solution, the computation time in Mathematica v. 12.1.1 (computer with an 8-core Intel Xeon W processor) was a few seconds, whereas the FE analysis with Abaqus took 78 min on the same computer. In the following figures, the kinematic response quantities are presented as a ratio to the static deflection of the slightly curved beam $w_S(0.5l)/p_0 = 5.24 \cdot 10^{-7}$ m^2/N, due to the load $p_S(x) = p_0\,(H(x) - H(x - l/2))$. The time t is normalized with the fundamental period T_1 of the with initial deflection, with $T_1 = 0.0145$ s. Fig. 8(a) shows the time history of the normalized deflection in the center of the slightly curved beam (black line) as well as the corresponding plane stress FE solution (red dashed line with black markers). In addition, this response variable is also depicted for the straight beam (blue line). In Fig. 8(b), the deflection along the beam length is shown for the time instant $t/T_1 = 5.225$. These figures demonstrate that, on the one hand, the presented beam theory reproduces the deflection very accurately and the deviation from the plane stress FE solution is negligible. The deflection is also asymmetric along the span due to the asymmetric load distribution. In comparison with the response of the straight beam, on the other hand, it becomes obvious what a large influence this very small initial deflection (1% of the span l) has on the deflection response: the response amplitude changes and a phase shift can be seen due to the change of the fundamental frequency.

The time history of the upper and lower interlayer slip Δu_1 and Δu_2 at the right end of the beam in Fig. 8(c) illustrates even more clearly the effect of the initial deflection on the response. With the straight beam, the amplitude of Δu_1 is about three times smaller than for the slightly curved beam. Fig. 8(d) shows that the upper and lower interlayer slips are the same in the interior of the beam, while they split in the sections of the beam ends where they have a different curvature. In contrast, for the straight symmetrically layered linear beam, the upper and lower interlayer slips are identical. Also these two figures illustrate

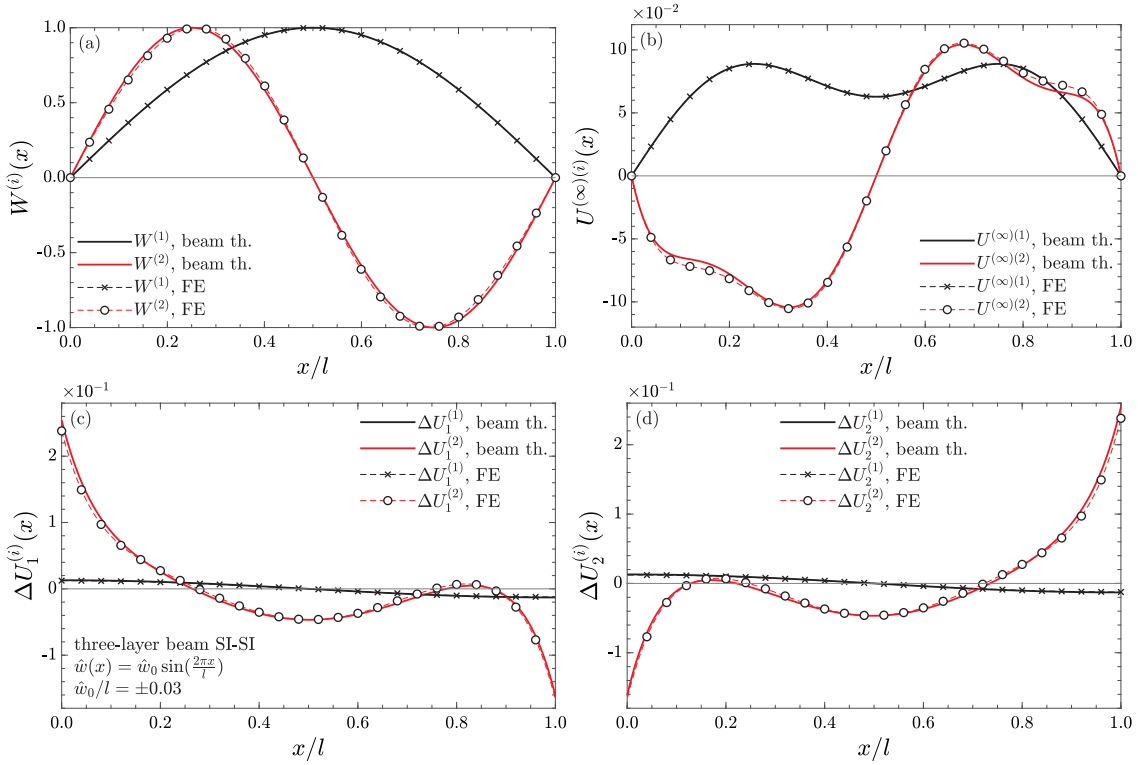

Fig. 7. First and second eigenfunction of the (a) deflection, (b) longitudinal displacement of the central axis, (c) upper interlayer slip, (d) lower interlayer slip. Initial deflection: sine wave. Three-layer beam. Soft-hinged horizontally immovably supported.

the excellent agreement of the response prediction of the beam theory and the FE analysis.

Fig. 8(e), which shows the normalized longitudinal displacement of the central axis $u^{(\infty)}$ at $x/l = 0.1l$ as a function of t/T_1, again proves the accuracy of beam theory for this example. The plot of $u^{(\infty)}$ versus x/l is included in Fig. 8(f). For the straight beam, $u^{(\infty)}(x,t) = 0$.

In addition, Fig. 9(a) shows the time history of the total normal force $N(0.5l)$ and the layerwise normal forces $N_1(0.5l)$, $N_2(0.5l)$ and $N_3(0.5l)$ in the center of the beam, normalized by the static overall axial force at midspan $N_S(0.5l)$ due to the static load $p_S(x)$ applied to the slightly curved beam, $N_S(0.5l)/p_0 = -1.362$ m. The distribution of the normal forces along the beam length at time $t/T_1 = 5.225$ in Fig. 9(b) demonstrates that the boundary conditions $N_1(x = 0, l) = N_3(x = 0, l) = 0$ and $N_2(x = 0, l) = N(x = 0, l)$ are fulfilled. Finally, Fig. 9(c) and (d) shows the time history of the overall bending moment $M(0.5l)$ and the partial bending moments $M_1(0.5l)$, $M_2(0.5l)$, $M_3(0.5l)$ at $x = 0.5l$ and their distribution over x/l at the same time instant, where these quantities are divided by the static overall axial bending moment at midspan $M_S(0.5l)$ of the beam with initial deflection, $M_S(0.5l)/p_0 = 4.891 \cdot 10^{-2}$ m^2.

4.4. Two-layer beam

In another application example, the natural frequencies, eigenfunctions and forced vibrations of a slightly curved two-layer beam with interlayer slip are sought with an approximation method. For the two-layer beam $EA_3 \equiv 0$, $EJ_3 \equiv 0$, $\rho_3 A_3 \equiv 0$, $K_{s2} \equiv 0$, $\Delta u_2 \equiv 0$, which also simplifies the boundary value problem at hand. Instead of four kinematic variables, the dynamic response is fully captured by the three kinematic variables w, $u^{(\infty)}$ and Δu_1.

Approximate procedure of analysis. The Galerkin method [44] is an efficient procedure used to solve the considered boundary value problem. To this end, the deflection $w(x,t)$ is approximated by the following Ritz approach [24],

$$w(x,t) \approx w^*(x,t) = \sum_{j=j_a}^{J} q_j(t)\phi_j(x) \ , \quad \phi_j(x) = \left(\frac{x}{l}\right)^j \left(1 - \frac{x}{l}\right)^{j_b} \tag{74}$$

with the shape functions $\phi_j(x)$ in form of a polynomial and the corresponding general coordinates $q_j(t)$. In the Galerkin method, the kinematic boundary conditions must be satisfied. This is achieved by a suitable choice of j_a for the actual geometric boundary condition for the deflection w at $x = 0$ and by a suitable choice of j_b for the actual geometric boundary condition for w at $x = l$ as follows [24]

free end (F) at $x = 0 : j_a = 0$ at $x = l : j_b = 0$ (75)

soft-hinged support (S),

hard-hinged support (H) at $x = 0 : j_a = 1$ at $x = l : j_b = 1$ (76)

clamped end (C) at $x = 0 : j_a = 2$ at $x = l : j_b = 2$ (77)

For example, if a cantilever is considered that is clamped at $x = 0$, $w(0) = w_{,x}(0) = 0$ must be satisfied, which is achieved by $j_a = 2$. At the free end at $x = l$ there are no geometric boundary conditions to be fulfilled, thus $j_b = 0$. The more series members J are included in Eq. (74), the better the dynamic boundary conditions and the dynamic response are approximated. It should be noted, however, that alternatively other methods such as generalized differential quadrature methods [49] could be used to solve this boundary value problem. For a recent application of this method to a similar problem see [32].

In the first step, the Ritz approximation of w Eq. (74) is inserted into the two equations of motion Eqs. (30) and (32) (with $EA_3 = 0$), which are subsequently solved for Δu_1 and $u^{(\infty)}$ taking into account the prevailing boundary conditions. For each end two boundary conditions must be fulfilled, i.e. for a soft-hinged support the boundary conditions Eqs. (37) and (39) (horizontally restraint, SI) or Eq. (41) (horizontally sliding, SM), for a hard-hinged support and clamped end the boundary conditions Eqs. (39) and (42) (horizontally restraint, HI and CI) or Eq. (41) (horizontally sliding, HM and CM), and for a free end (F)

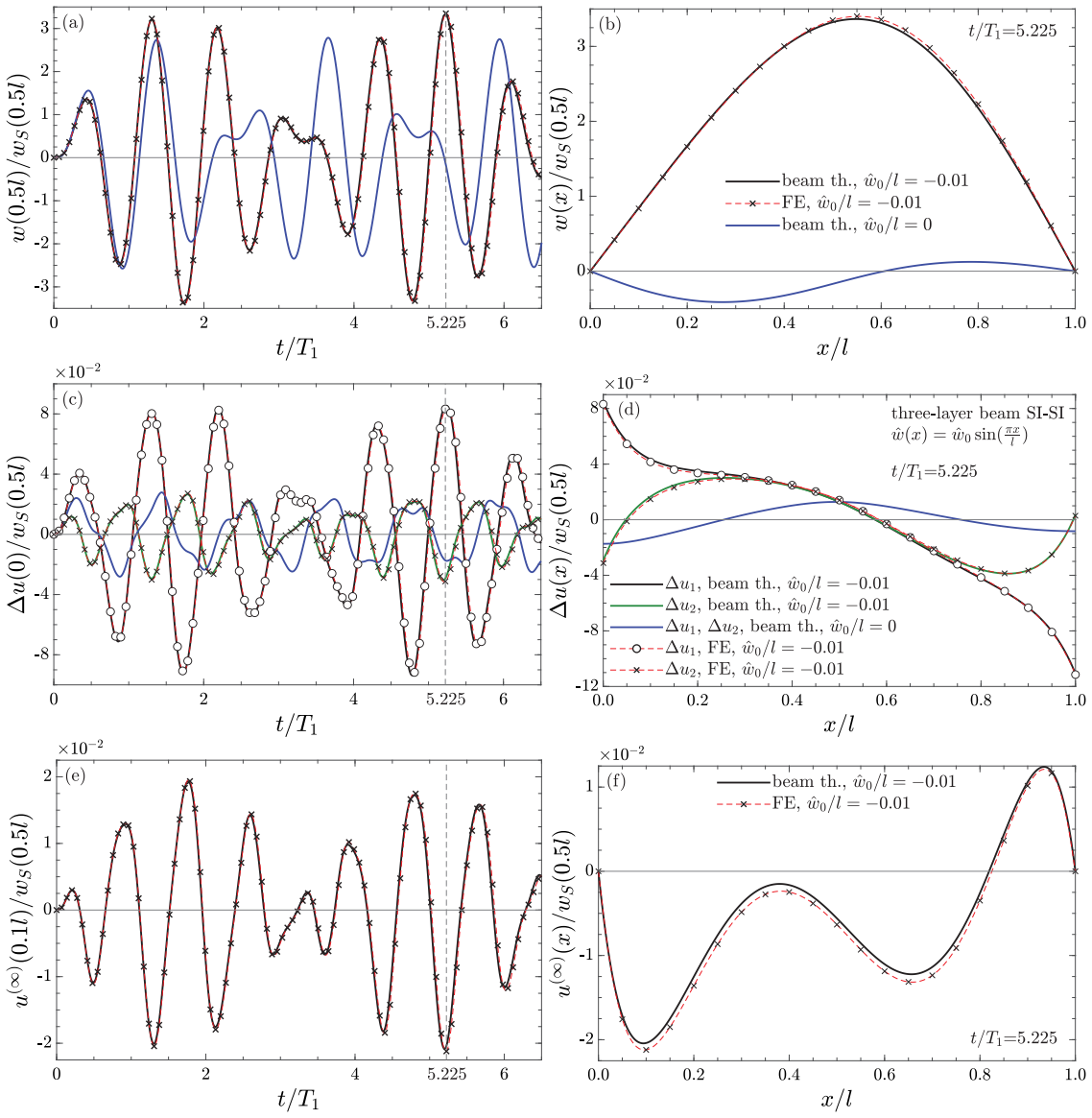

Fig. 8. Time history of the kinematic variables at midspan (left column) and their distribution along the beam axis at a given time instant (right column): (a,b) deflection, (c,d) upper and lower interlayer slip, (e,f) longitudinal displacement of the central axis. Three-layer beam with initial deflection and straight axis, respectively. Soft-hinged horizontally immovably supported. (For interpretation of the references to color in this figure legend, the reader is referred to the web version of this article.)

the boundary conditions Eqs. (37) and (41). The solution can be found analytically for instance with the software packages Mathematica [50] or Maple [51]. Δu_1 and $u^{(\infty)}$ are then available as a function of the generalized coordinates q_j, $j = j_a, \dots, J$, and subsequently denoted as Δu_1^* and $u^{(\infty)*}$,

$$\Delta u_1^*(x,t) = \sum_{j=j_a}^{J} q_j(t)\bar{\phi}_j(x)\ , \quad u^{(\infty)*}(x,t) = \sum_{j=j_a}^{J} q_j(t)\bar{\bar{\phi}}_j(x) \tag{78}$$

where $\bar{\phi}_j(x)$ and $\bar{\bar{\phi}}_j(x)$ denote the functions approximating the shape of u_1 and $u^{(\infty)}$, respectively, resulting from the procedure described above.

The first derivatives of w^*, Δu_1^* and $u^{(\infty)*}$ with respect to x are subsequently substituted in the integral representation of the normal force $N(t)$ according to Eq. (31), which is then also a function of q_j (referred to as N^*). Eventually, the applicable derivatives of w^*, Δu_1^* and $u^{(\infty)*}$ with respect to t and x as well as N^* are inserted into the equation of motion Eq. (28), and according to the Galerkin method [44], multiplied by the shape function ϕ_k and integrated over the span l. This procedure is repeated $(J - j_a + 1)$ times for each shape function. In general, the chosen set of shape functions do not satisfy the dynamic boundary conditions, and thus the work of the boundary forces must be added [44],

$$\int_0^l \Big(\mu\ddot{w}^* + EJ_\infty w^*_{,xxxx} + EA_1 z_1 \Delta u^*_{1,xxx} - N^*\hat{w}_{,xx} - p\Big)\phi_i dx - M_b^*(\phi_{i,x})_b + \big((M^*_{,x})_b + N_b^*(\hat{w}_{,x})_b\big)(\phi_i)_b = 0\ , \quad i = j_a, \dots, J \tag{79}$$

These equations are integrated by parts twice with respect to x in order to reduce the order of the derivatives with respect to x by two. Since in general the shape functions violate the dynamic boundary conditions, the negative work of the boundary forces appears in the resulting set of equations, which however cancels out with the positive work of the boundary forces apparent in Eq. (79),

$$\int_0^l \Big(\Big(EJ_\infty w^*_{,xx} + EA_1 z_1 \Delta u^*_{1,x}\Big)\phi_{i,xx} + N^*\hat{w}_{,x}\phi_{i,x} + \big(\mu\ddot{w}^* - p\big)\phi_i\Big)dx = 0\ , \quad i = j_a, \dots, J \tag{80}$$

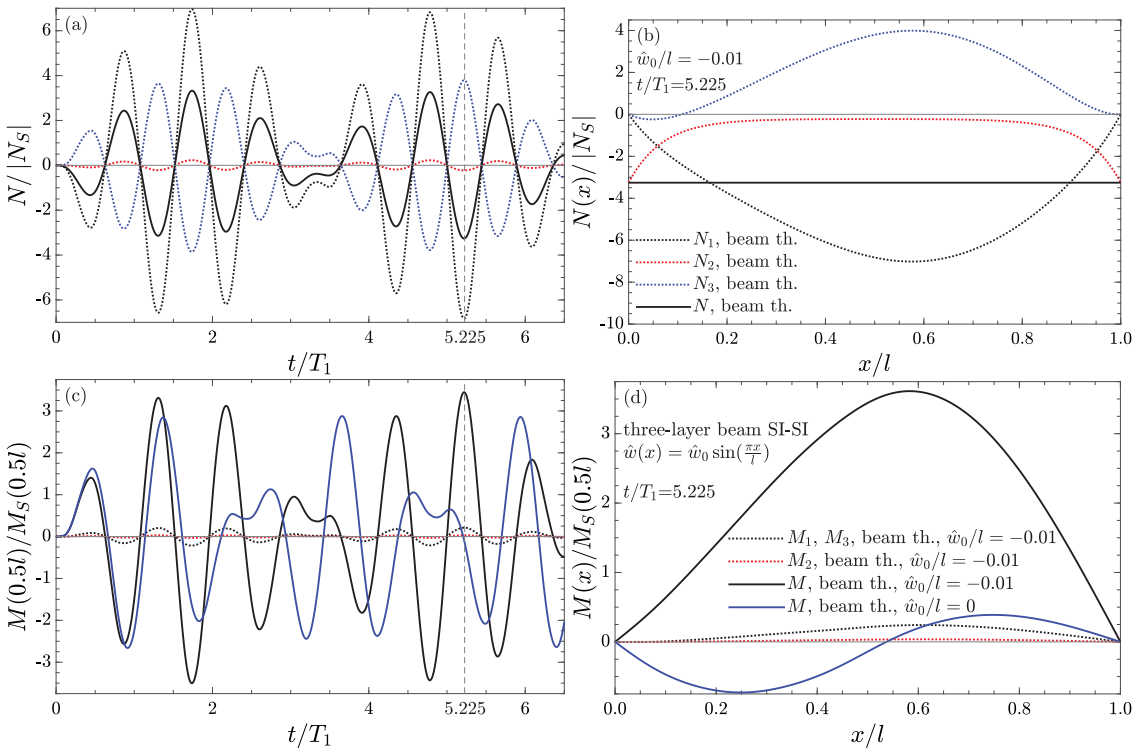

Fig. 9. Time history of the overall and layerwise internal forces (left) and their distribution along the beam axis at a given time instant (right). (a,b) axial forces, (c,d) bending moments. Three-layer beam with initial deflection and straight axis, respectively. Soft-hinged horizontally immovably supported.

The evaluation of the integrals yields $(J - j_a + 1)$ ordinary coupled differential equations in $q_j(t)$,

$$\sum_{j=j_a}^{J} \left(m^*_{ij} \ddot{q}_j + k^*_{ij} q_j \right) = p^*_i \ , \quad i = j_a, \dots, J \tag{81}$$

with

$$\begin{aligned} m^*_{ij} &= \mu \int_0^l \phi_i(x)\phi_j(x)dx \ , \quad p^*_i(t) = \int_0^l p(x,t)\phi_i(x)dx \ , \\ k^*_{ij} &= \int_0^l \Big(\left(EJ_\infty \phi_{j,xx}(x) + EA_1 z_1 \bar{\phi}_{j,x}(x) \right) \phi_{i,xx}(x) \\ &\quad - N_s^{(j)*} \hat{w}_{,xx}(x)\phi_i(x) \Big) dx \ , \\ N_s^{(j)*} &= \frac{EA_e}{l} \int_0^l \left(\bar{\bar{\phi}}_{j,x}(x) + \phi_{j,x}(x)\hat{w}_{,x}(x) \right) dx - \frac{EA_1}{l} \int_0^l \bar{\phi}_{j,x}(x)dx \end{aligned} \tag{82}$$

or alternatively in matrix notation

$$\mathbf{M}^*\ddot{\mathbf{q}} + \mathbf{K}^*\mathbf{q} = \mathbf{p}^* \ , \quad \mathbf{q} = \{q_{ja}, \dots, q_j, \dots, q_L\}^\mathsf{T} \ , \quad \mathbf{p}^* = \{p^*_{ja}, \dots, p^*_j, \dots, p^*_L\}^\mathsf{T} \tag{83}$$

with $\mathbf{M}^*$ denoting the mass matrix composed of the mass coefficients m^*_{ij} and $\mathbf{K}^*$ the stiffness matrix composed of the stiffness coefficients k^*_{ij}. Eq. (83) can be solved for $q_j(t)$, $j = j_a, \dots, J$, by numerical standard solvers.

It is, however, advantageous to decouple this set of coupled linear equations with the means of modal analysis, since in the resulting modal equations in the form of the SDOF oscillator damping can be taken into account simply by adding it modally as in an SDOF system. The $(J - j_a + 1)$ natural angular frequencies ω^*_j and eigenvectors $\mathbf{\Phi}^*_j$ of the system discretized with the Ritz approach Eq. (74), on which the modal analysis is based, follow from

$$\left(\mathbf{K}^* - \omega^{*2}\mathbf{M}^* \right) \mathbf{\Phi}^* = \mathbf{0} \tag{84}$$

An approximation of the ith eigenfunctions $W^{(i)}(x)$, $\Delta U_1^{(i)}(x)$, $U^{\infty(i)}$ is obtained by substituting the components $\mathbf{\Phi}^{*(i)}_j$ $(j = ja, \dots, J)$ of the ith eigenvector $\mathbf{\Phi}^*_i$ in Eqs. (74) and (78) instead of the generalized coordinates q_j,

$$\begin{aligned} W^{(j)*}(x) &= \sum_{j=j_a}^{J} \mathbf{\Phi}^{*(i)}_j \phi_j(x) \ , \quad \Delta U_1^{(j)*}(x) = \sum_{j=j_a}^{J} \mathbf{\Phi}^{*(i)}_j \bar{\phi}_j(x) \ , \\ U^{\infty(j)*}(x) &= \sum_{j=j_a}^{J} \mathbf{\Phi}^{*(i)}_j \bar{\bar{\phi}}_j(x) \end{aligned} \tag{85}$$

Inserting the modal expansion of $\mathbf{q}$ with respect to the eigenvectors $\mathbf{\Phi}^*_i$,

$$\mathbf{q}(t) = \sum_{i=1}^{J-j_a+1} Y^\circ_i(t)\mathbf{\Phi}^*_i \tag{86}$$

into Eq. (83) and successive pre-multiplication with $\mathbf{\Phi}^{*\mathsf{T}}_i$ leads to the modal oscillator equations in Y°_i,

$$\begin{aligned} &\ddot{Y}^\circ_i + 2\zeta_i\omega^*_i\dot{Y}^\circ_i + \omega^{*2}_i Y^\circ_i = \frac{p^\circ_i}{m^\circ_i} \ , \quad p^\circ_i = \mathbf{\Phi}^{*\mathsf{T}}_i \mathbf{p}^* \ , \\ &m^\circ_i = \mathbf{\Phi}^{*\mathsf{T}}_i \mathbf{M}^* \mathbf{\Phi}^*_i \ , \quad i = 1, \dots, J - j_a + 1 \end{aligned} \tag{87}$$

which can be solved with the standard methods of linear vibration theory. As described before, damping was added modally in Eq. (87). Substituting of $Y^*_i(t)$, $i = 1, \dots, J - j_a + 1$, into Eq. (86) yields the generalized coordinates q_j, $j = j_a, \dots, J$, that are subsequently inserted into the expressions for w^* (Eq. (74)), Δu^*_1 and $u^{(\infty)*}$ (Eq. (78)), which approximate the kinematic variables w, Δu_1 and $u^{(\infty)}$.

4.5. Two-layer beam example problems

In the following application examples, two-layer beams with the following dimensions are considered: Length $l = 1.0$ m, cross-sectional dimensions of the two layers $h_1 = 0.004$ m, $h_2 = 0.0261$ m, $b_1 = b_2 = 0.1$ m. The material parameters are as follows: $E_1 = 7.0 \cdot 10^{10}$ N/m^2, $E_2 = 1.0 \cdot 10^{10}$ N/m^2, $K_{s1} = 1.0 \cdot 10^9$ N/m^2, $\rho_1 = 2700$ kg/m, $\rho_2 =$

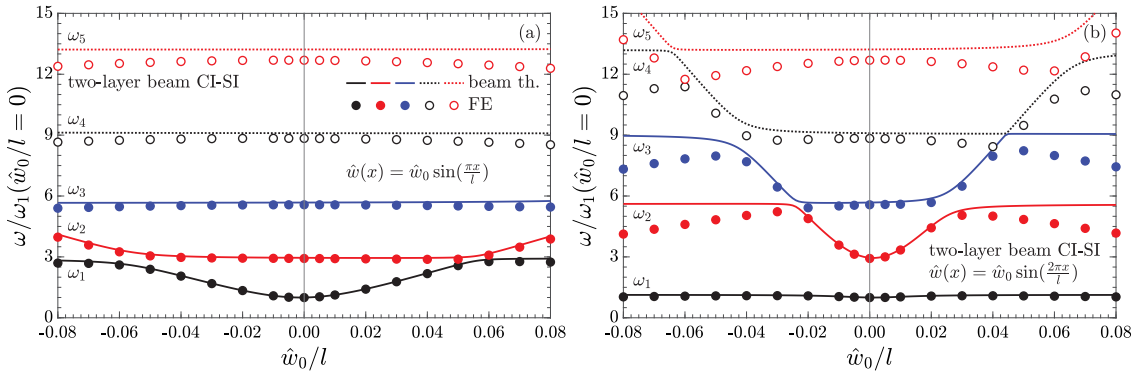

Fig. 10. First five natural frequencies as a function of the normalized amplitude of the initial deflection. Initial deflection (a) sine half-wave, (b) sine wave. Two-layer beam. Clamped-soft-hinged horizontally immovably supported.

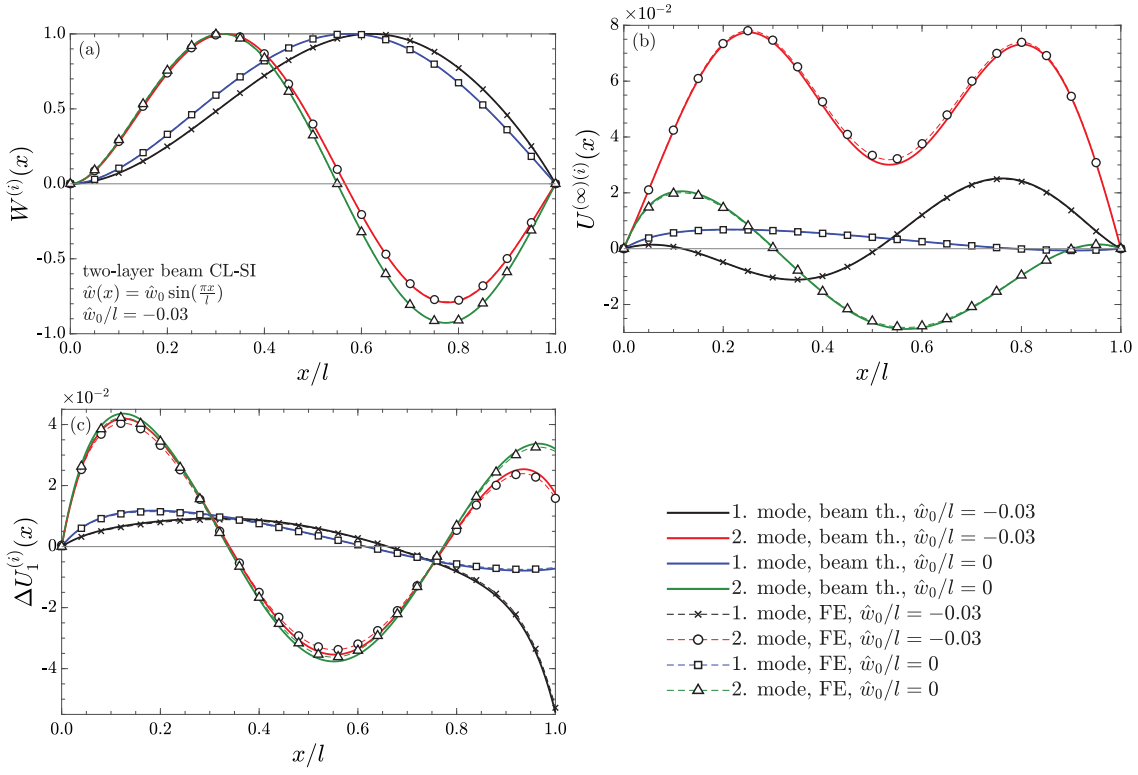

Fig. 11. First and second eigenfunction of the (a) deflection, (b) longitudinal displacement of the central axis, (c) interlayer slip. Initial deflection: sine half-wave. Two-layer beam. Clamped-soft-hinged horizontally immovably supported.

1000 kg/m. These parameters result in a layer interaction parameter α for the two-layer beam (see e.g. [2]),

$$\alpha = \left(K_{s1} \left(\frac{EA_e}{EA_1 EA_2} + \frac{(h_1/2 + h_2/2)^2}{EJ_0} \right) \right)^{1/2} \tag{88}$$

times length l of $\alpha l = 15.0$. On the left side the beam is clamped, on the right side soft-hinged supported. The horizontal movement is constrained on both supports (CI-SI). Convergence studies have shown that the 11 shape functions approximate sufficiently accurately the response of the present examples. The results of the proposed beam theory are again contrasted with finite element solutions assuming a plane stress state. The finite element models created in Abaqus have 34,910 degrees of freedom. In these models, the thickness of the cohesive elements of the interlayer is 0.0001 m as for the three-layer beams. The height h_2 is reduced by this value so that the total height of the beams remains the same as in the beam models.

In the first example, the first five natural frequencies $\omega_1, \omega_2, \omega_3, \omega_4, \omega_5$ of the beam are analyzed, whose initial deflection follows a sine half-wave: $\hat{w}(x) = \hat{w}_0 \sin(\pi x/l)$. Due to the asymmetric layer arrangement, the modal parameters also depend on the sign of the initial deflection (in contrast to the symmetrically layered beam). Therefore, in Fig. 10(a), the natural frequencies are depicted as a function of the maximum initial deflection (normalized by the length l) in the range $-0.08 \le \hat{w}_0/l \le 0.08$. Here, the natural frequencies are divided by the fundamental frequency of the straight beam $\omega_1(\hat{w}_0 = 0) = 496.6$ rad/s. The comparison of the beam solution shown with solid lines with the results of the FE analysis (represented by markers) demonstrates that in the whole range of $\hat{w}_0/l$ the first four natural angular frequencies are reproduced very well by the presented beam theory. For the fifth natural frequency, the largest deviation from the "exact" FE solution is 7.73%, which occurs at a relatively large initial deflection $\hat{w}_0$ of 8% of the beam length. Up to a initial deflection amplitude $\hat{w}_0$ of ±5% of the beam length, the initial deflection mainly affects the fundamental frequency ω_1, which increases in this range with increasing $\hat{w}_0/l$. The reason for this is that the initial deflection has like the first eigenfunction for the deflection no node, as can be seen in Fig. 11(a) for the beam

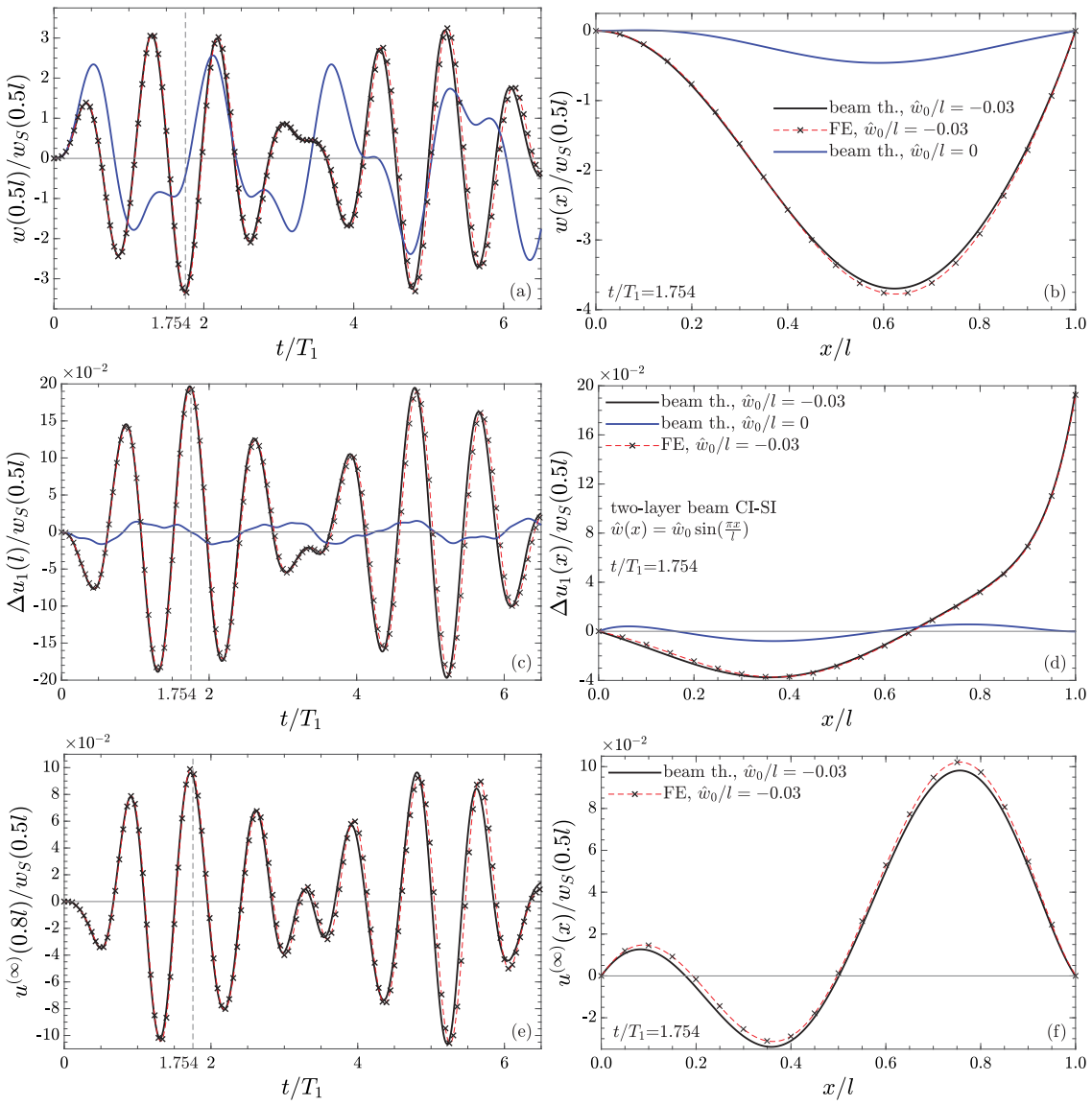

Fig. 12. Time history of the kinematic variables at midspan (left column) and their distribution along the beam axis at a given time instant (right column): (a,b) deflection, (c,d) interlayer slip, (e,f) longitudinal displacement of the central axis. Two-layer beam with initial deflection and straight axis, respectively. Left end clamped, right end soft-hinged horizontally immovably supported.

with the initial deflection $\hat{w}_0/l = -0.03$. For initial deflection amplitude ratios $|\hat{w}_0/l| > 0.05$, the second natural frequency increases with $\hat{w}_0$ and the first frequency has approximately the value of the second natural frequency of the straight beam.

Fig. 11(a) shows the first and second eigenfunctions $W^{(1)}$ and $W^{(2)}$ for the deflection of the beam with initial deflection $\hat{w}_0/l = -0.03$ and the straight beam, respectively. As observed, these eigenfunctions of the two beams have a similar shape, but their maxima shift to the right due to the initial deflection. The initial deflection has a much more significant influence on the first two eigenfunctions $U^{(\infty)(1)}$ and $U^{(\infty)(2)}$ of the longitudinal displacement of the beam axis, as can be seen in Fig. 11(b). While the first eigenfunction $U^{(\infty)(1)}$ of the slightly curved beam has two nodes, $U^{(\infty)(1)}$ of the straight beam has only one. For the eigenfunctions of the interlayer slip $\Delta U_1^{(1)}$ and $\Delta U_1^{(2)}$, especially the first one is influenced by the initial deflection, as Fig. 11(c) shows, the second eigenfunction is visibly different only in the region of the right soft-hinged support. The also shown solutions from the plane stress FE analyses are practically identical with all considered eigenfunctions of the beam theory.

When the beam has an initial deflection in the form of a sine wave, $\hat{w}(x) = \hat{w}_0 \sin(2\pi x/l)$, which has a node just like the second eigenfunction for the deflection, the first natural angular ω_1 is hardly affected by this initial deflection, as can be seen from Fig. 10(b). Up to a initial deflection of $\hat{w}_0/l = \pm 0.025$ the second natural frequency ω_2 increases with $\hat{w}_0/l$, in the range $0.025 < \hat{w}_0/l < 0.045$ the third natural frequency increases and so on. The comparison with the FE solution shows that the fundamental frequency ω_1 can be estimated very well by the beam theory in the whole considered range of initial deflection amplitude, while the second, third and fourth natural angular frequencies are well reproduced up to a ratio of $\hat{w}_0/l \approx \pm 0.03$. As described before, the second natural angular frequency ω_2 increases up to a initial deflection of $|\hat{w}_0|/l \approx 0.025$. While according to the beam theory this frequency remains constant for $|\hat{w}_0|/l > 0.025$, the plane stress FE analysis shows that ω_2 actually decreases again when $|\hat{w}_0|/l > 0.025$.

Finally, the forced vibration response of the two-layer beam is discussed, whose beam axis is slightly curved in the form of a sine half-wave, $\hat{w}(x) = \hat{w}_0 \sin(\pi x/l)$ with $\hat{w}_0 = -0.03$ m, and is induced by a time-harmonic uniform load $p(x,t) = p_0 \sin(\nu t)$ switched on at time $t = 0$. The excitation frequency ν is 1.3 times the fundamental frequency ω_1

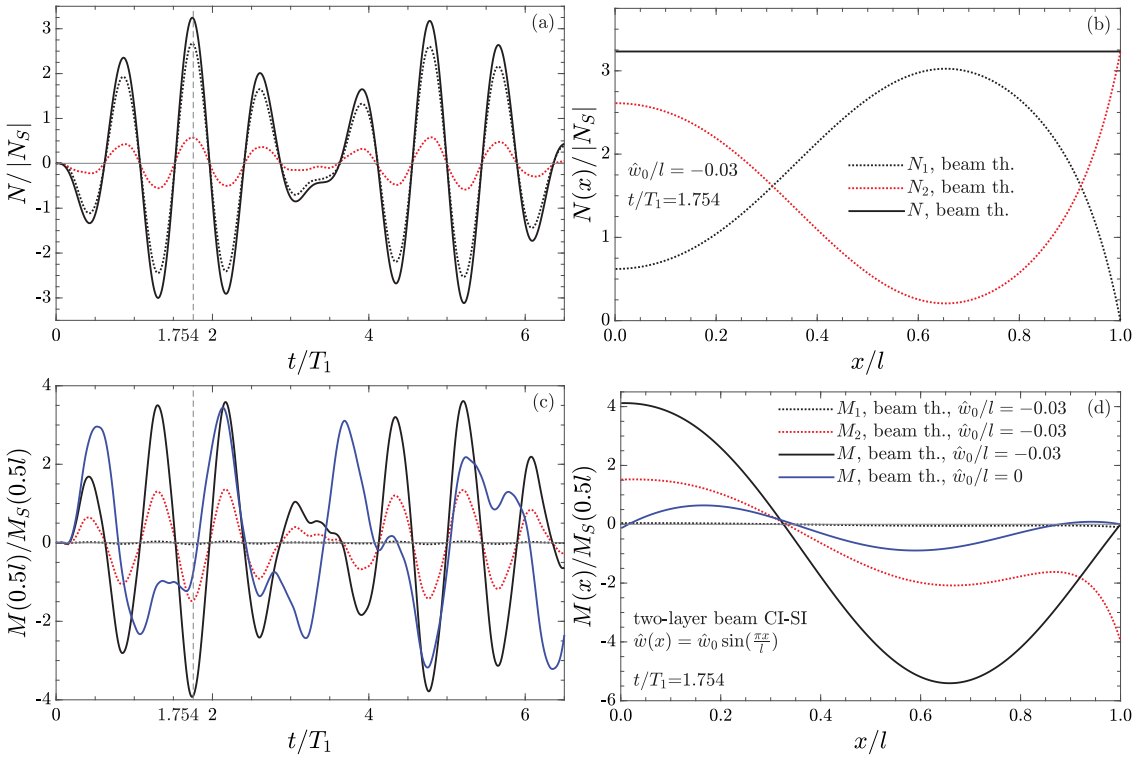

Fig. 13. Time history of the overall and layerwise internal forces (left) and their distribution along the beam axis at a given time instant (right). (a,b) axial forces, (c,d) bending moments. Two-layer beam with initial deflection and straight axis, respectively. Left end clamped, right end soft-hinged horizontally immovably supported.

of the beam with initial deflection. The kinematic variables shown in Fig. 12 are normalized by the static deflection of the slightly curved beam at midspan, $w_S(x = 0.5l)$, due to the load $p(x) = p_0$, with $w_S(0.5l)/p_0 = 4.53{\cdot}10^{-7}$ m^2/N. The time t is also made non-dimensional by division with the fundamental period of the slightly curved beam $T_1 = 7.47 \cdot 10^{-3}$ s. The plots in the left column of this figure show the time histories of the deflection at midspan (Fig. 12(a)), the interlayer slip at the right end of the beam (Fig. 12(c)), and the horizontal displacement of the central axis at $x/l = 0.8l$. The plots in the right column depict the distribution of these quantities over x/l at time $t/T_1 = 1.754$ (Fig. 12(b,d,e)). The comparison of the beam solution with the result of the plane stress FE analysis demonstrates once more a very good agreement with hardly visible deviations. It should be noted here that in this example, the computational time for the FE analysis with Abaqus was about 205 min, while the solution with beam theory with Mathematica on the same computer (8-core Intel Xeon W processor) was found in less than a minute.

In contrast, the kinematic response of the straight beam deviates strongly from that of the slightly curved one, as can also be seen in Fig. 12. For instance, the maximum value of the interlayer slip at the right support is less than 10% of the one of the straight beam, see Fig. 12(c). Moreover, the horizontal displacement of the central axis of the straight beam is zero, Fig. 12(e).

Finally, Fig. 13 shows the normal force, Fig. 13(a,b), and the moment, Fig. 13(c,d), of the two layers as well as the overall beam. The normal forces are normalized with the overall normal force $N_S(0.5l)$ in the beam center due to the static load with $N_S(0.5l)/p_0 = 2.851$ m, the moments with the overall moment $M_S(0.5l)$ in the beam center subjected this static load with $M_S(0.5l)/p_0 = 0.01775$ m^2. Fig. 13(d) shows that at the right support the total moment M is virtually zero, i.e. the selected number of $J = 11$ shape functions $\varphi_j(x)$ is sufficient to approximate the dynamic boundary condition $M(l,t) = 0$ accurately.

5. Summary and conclusions

Based on the fundamental linearized kinematic relations, a layerwise application of Euler–Bernoulli theory and a linear constitutive law for the interlayer slip, the equations of motion and boundary conditions of slightly curved composite beams with flexibly bonded layers were derived using Hamilton's principle. The resulting initial–boundary value problem was solved analytically for the symmetrically layered three-layer beam soft-hinged at both ends. When both supports are horizontally immovable and the initial deflection is proportional to one eigenfunction of the deflection of the straight beam, then the eigenfunctions of the deflection of the straight beam are equal to those of the slightly curved member. Compared to the straight beam, the initial deflection leads to an increase in that natural frequency whose mode is proportional to the initial deflection, and the corresponding eigenfunctions of the upper and lower interlayer slip are different. The other natural frequencies coincide with those of the straight beam, and the natural functions of the upper and lower interlayer slip are identical and also correspond to those of the straight member. Unlike the straight beam, the eigenfunctions of the longitudinal displacement of the beam axis are non-zero.

When one of the two supports of the slightly curved member slides horizontally, the natural frequencies, the eigenfunctions of the deflection and the interlayer slips correspond to those of the straight beam. However, in contrast to the straight beam, the eigenfunction of the longitudinal displacement of the central axis, whose mode is proportional to the initial deflection, is non-zero.

Since for arbitrary boundary conditions of the considered slightly curved composite beams with arbitrary arrangement of the layers the analytical solution of the present boundary value problem is either very costly or not possible, a numerical procedure for the computation of the natural frequencies, eigenfunctions and forced vibration response based on Galerkin's method is adapted on the example of a two-layer beam with interlayer slip.

Several application examples demonstrate the large influence of initial deflection on the dynamics of slender composite beams whose layers are flexibly connected. In addition, finite element analyses were performed where, assuming a plane stress state, the considered structures were discretized with continuum elements. The results of the

presented beam theory are in excellent agreement with the results of these finite element analyses for a wide range of initial deflection amplitude, which confirms the accuracy of this theory. This comparison also illustrates the efficiency of the beam theory in comparison with the much more computational demanding and time consuming finite element analyses of the continuum model.

CRediT authorship contribution statement

Christoph Adam: Writing – review & editing, Writing – original draft, Supervision, Resources, Investigation, Formal analysis, Conceptualization. **Dominik Ladurner:** Writing – review & editing, Validation, Software, Investigation, Formal analysis. **Thomas Furtmüller:** Writing – review & editing, Validation, Supervision.

Declaration of competing interest

The authors declare that they have no known competing financial interests or personal relationships that could have appeared to influence the work reported in this paper.

Data availability

The authors are unable or have chosen not to specify which data has been used.

References

[1] U.A. Girhammar, V.K.A. Gopu, Composite beam-columns with interlayer slip-exact analysis, J. Struct. Eng. 119 (1993) 1265–1282.

[2] U.A. Girhammar, D.H. Pan, Exact static analysis of partially composite beams and beam-columns, Int. J. Mech. Sci. 49 (2) (2007) 239–255, http://dx.doi.org/10.1016/j.ijmecsci.2006.07.005, URL http://www.sciencedirect.com/science/article/pii/S0020740306001512.

[3] S. Schnabl, I. Planinc, M. Saje, B. Čas, G. Turk, An analytical model of layered continuous beams with partial interaction, Struct. Eng. Mech. 22 (2006) 263–278.

[4] A.F. Siciliano, L. Š.kec, G. Jelenić, Closed-form solutions for modelling the rotational stiffness of continuous and discontinuous compliant interfaces in two-layer Timoshenko beams, Acta Mech. 232 (7) (2021) 2793–2824, http://dx.doi.org/10.1007/s00707-021-02958-x.

[5] J. Gahleitner, J. Schoeftner, A two-layer beam model with interlayer slip based on two-dimensional elasticity, Compos. Struct. 274 (2021) 114283, http://dx.doi.org/10.1016/j.compstruct.2021.114283, URL https://www.sciencedirect.com/science/article/pii/S0263822321007455.

[6] N. Challamel, U.A. Girhammar, Variationally-based theories for buckling of partial composite beam–columns including shear and axial effects, Eng. Struct. 33 (8) (2011) 2297–2319, http://dx.doi.org/10.1016/j.engstruct.2011.04.004, URL https://www.sciencedirect.com/science/article/pii/S0141029611001520.

[7] S. Schnabl, I. Planinc, The effect of longitudinal cracks on buckling loads of columns, Arch. Appl. Mech. 89 (5) (2019) 847–858, http://dx.doi.org/10.1007/s00419-018-1426-2.

[8] H.-J. Kim, K. Yoon, P.-S. Lee, Continuum mechanics based beam elements for linear and nonlinear analyses of multi-layered composite beams with interlayer slips, Compos. Struct. 235 (2020) 111740, http://dx.doi.org/10.1016/j.compstruct.2019.111740, URL https://www.sciencedirect.com/science/article/pii/S0263822319309110.

[9] A. Kroflič, M. Saje, I. Planinc, Non-linear analysis of two-layer beams with interlayer slip and uplift, Comput. Struct. 89 (23) (2011) 2414–2424, http://dx.doi.org/10.1016/j.compstruc.2011.06.007, URL https://www.sciencedirect.com/science/article/pii/S0045794911001921.

[10] M.A. Uddin, A.H. Sheikh, D. Brown, T. Bennett, B. Uy, A higher order model for inelastic response of composite beams with interfacial slip using a dissipation based arc-length method, Eng. Struct. 139 (2017) 120–134.

[11] U.A. Girhammar, D. Pan, Dynamic analysis of composite members with interlayer slip, Int. J. Solids Struct. 30 (1993) 797–823.

[12] C. Adam, R. Heuer, A. Jeschko, Flexural vibrations of elastic composite beams with interlayer slip, Acta Mech. 125 (1997) 17–30.

[13] C. Adam, R. Heuer, A. Raue, F. Ziegler, Thermally induced vibrations of composite beams with interlayer slip, J. Therm. Stress. 23 (2000) 747–772.

[14] R. Heuer, Thermo-piezoelectric flexural vibrations of viscoelastic panel-type laminates with interlayer slip, Acta Mech. 181 (3) (2006) 129–138, http://dx.doi.org/10.1007/s00707-005-0299-y.

[15] U.A. Girhammar, D.H. Pan, A. Gustafsson, Exact dynamic analysis of composite beams with partial interaction, Int. J. Mech. Sci. 51 (8) (2009) 565–582, http://dx.doi.org/10.1016/j.ijmecsci.2009.06.004, URL https://www.sciencedirect.com/science/article/pii/S0020740309001052.

[16] Q.-H. Nguyen, M. Hjiaj, P. Le Grognec, Analytical approach for free vibration analysis of two-layer timoshenko beams with interlayer slip, J. Sound Vib. 331 (12) (2012) 2949–2961.

[17] C. Adam, T. Furtmüller, Flexural vibrations of geometrically nonlinear composite beams with interlayer slip, Acta Mech. 231 (1) (2020) 251–271, http://dx.doi.org/10.1007/s00707-019-02528-2.

[18] W.Y. Tseng, J. Dugundji, Nonlnear vibrations of a buckled beam under harmonic excitation, J. Appl. Mech. 38 (2) (1971) 467–476.

[19] C. Adam, F. Ziegler, Moderately large forced oblique vibrations of elastic-viscoplastic deteriorating slightly curved beams, Arch. Appl. Mech. 67 (6) (1997) 375–392.

[20] Y. Si-Qin, M. Xiao-Ye, D. Hu, J.-C. Ji, C. Li-Qun, Nonlinear vibrations of a slightly curved beam with nonlinear boundary conditions, Int. J. Mech. Sci. 168 (2020) 105294.

[21] X. Xu, B. Karami, D. Shahsavari, Time-dependent behavior of porous curved nanobeam, Internat. J. Engrg. Sci. 160 (2021) 103455, http://dx.doi.org/10.1016/j.ijengsci.2021.103455, URL https://www.sciencedirect.com/science/article/pii/S0020722521000021.

[22] G.-L. She, H.-B. Liu, B. Karami, Resonance analysis of composite curved microbeams reinforced with graphene nanoplatelets, Thin-Walled Struct. 160 (2021) 107407, http://dx.doi.org/10.1016/j.tws.2020.107407, URL https://www.sciencedirect.com/science/article/pii/S0263823120312702.

[23] P. Talebizadehsardari, A. Eyvazian, M. Asmael, B. Karami, D. Shahsavari, R.B. Mahani, Static bending analysis of functionally graded polymer composite curved beams reinforced with carbon nanotubes, Thin-Walled Struct. 157 (2020) 107139, http://dx.doi.org/10.1016/j.tws.2020.107139, URL https://www.sciencedirect.com/science/article/pii/S0263823120310120.

[24] M. Qatu, In-plane vibration of slightly curved laminated composite beams, J. Sound Vib. 159 (2) (1992) 327–338, http://dx.doi.org/10.1016/0022-460X(92)90039-Z, URL https://www.sciencedirect.com/science/article/pii/0022460X92900039Z.

[25] K. Susanto, Vibration analysis of piezoelectric laminated slightly curved beams using distributed transfer function method, Int. J. Solids Struct. 46 (6) (2009) 1564–1573.

[26] L. Jun, R. Guangwei, P. Jin, L. Xiaobin, W. Weiguo, Free vibration analysis of a laminated shallow curved beam based on trigonometric shear deformation theory, Mech. Based Des. Struct. Mach. 42 (1) (2014) 111–129, http://dx.doi.org/10.1080/15397734.2013.846224, arXiv:https://doi.org/10.1080/15397734.2013.846224.

[27] P.V. Avhad, A.S. Sayyad, On the static deformation of FG sandwich beams curved in elevation using a new higher order beam theory, Sādhanā 45 (1) (2020) 188, http://dx.doi.org/10.1007/s12046-020-01425-y.

[28] P.V. Avhad, A.S. Sayyad, On the deformation of laminated composite and sandwich curved beams, Curved Layer. Struct. 9 (1) (2022) 1–12, http://dx.doi.org/10.1515/cls-2022-0001, [cited 2022-06-14].

[29] A.S. Sayyad, P.V. Avhad, A new higher order shear and normal deformation theory for the free vibration analysis of sandwich curved beams, Compos. Struct. 280 (2022) 114948, http://dx.doi.org/10.1016/j.compstruct.2021.114948, URL https://www.sciencedirect.com/science/article/pii/S0263822321013799.

[30] B. Karami, M. Janghorban, H. Fahham, Forced vibration analysis of anisotropic curved panels via a quasi-3D model in orthogonal curvilinear coordinate, Thin-Walled Struct. 175 (2022) 109254, http://dx.doi.org/10.1016/j.tws.2022.109254, URL https://www.sciencedirect.com/science/article/pii/S0263823122002014.

[31] H. Berghouti, E. Adda Bedia, A. Benkhedda, A. Tounsi, Vibration analysis of nonlocal porous nanobeams made of functionally graded material, Adv. Nano Res. 7 (5) (2019) 351–364.

[32] B. Karami, M. Janghorban, H. Fahham, On the stress analysis of anisotropic curved panels, Internat. J. Engrg. Sci. 172 (2022) 103625, http://dx.doi.org/10.1016/j.ijengsci.2022.103625, URL https://www.sciencedirect.com/science/article/pii/S0020722522000027.

[33] J. Song, B. Karami, D. Shahsavari, O. Civalek, Wave dispersion characteristics of graphene reinforced nanocomposite curved viscoelastic panels, Compos. Struct. 277 (2021) 114648, http://dx.doi.org/10.1016/j.compstruct.2021.114648, URL https://www.sciencedirect.com/science/article/pii/S0263822321011077.

[34] X. Liu, B. Karami, D. Shahsavari, O. Civalek, Elastic wave characteristics in damped laminated composite nano-scaled shells with different panel shapes, Compos. Struct. 267 (2021) 113924, http://dx.doi.org/10.1016/j.compstruct.2021.113924, URL https://www.sciencedirect.com/science/article/pii/S0263822321003846.

[35] A. Eyvazian, D. Shahsavari, B. Karami, On the dynamic of graphene reinforced nanocomposite cylindrical shells subjected to a moving harmonic load, Internat. J. Engrg. Sci. 154 (2020) 103339, http://dx.doi.org/10.1016/j.ijengsci.2020.103339, URL https://www.sciencedirect.com/science/article/pii/S0020722520301270.

[36] B. Karami, D. Shahsavari, On the forced resonant vibration analysis of functionally graded polymer composite doubly-curved nanoshells reinforced with graphene-nanoplatelets, Comput. Methods Appl. Mech. Engrg. 359 (2020) 112767, http://dx.doi.org/10.1016/j.cma.2019.112767, URL https://www.sciencedirect.com/science/article/pii/S0045782519306590.

[37] X. Xu, D. Shahsavari, B. Karami, On the forced mechanics of doubly-curved nanoshell, Internat. J. Engrg. Sci. 168 (2021) 103538, http://dx.doi.org/10.1016/j.ijengsci.2021.103538, URL https://www.sciencedirect.com/science/article/pii/S0020722521000859.

[38] X. Xu, B. Karami, M. Janghorban, On the dynamics of nanoshells, Internat. J. Engrg. Sci. 158 (2021) 103431, http://dx.doi.org/10.1016/j.ijengsci.2020.103431, URL https://www.sciencedirect.com/science/article/pii/S0020722520302184.

[39] M. Hajianmaleki, M.S. Qatu, Vibrations of straight and curved composite beams: A review, Compos. Struct. 100 (C) (2013) 218–232.

[40] I. Ecsedi, A.J. Lengyel, Curved composite beam with interlayer slip loaded by radial load, Curved Layer. Struct. 2 (1) (2015) 25–40.

[41] Á.J. Lengyel, Static and Dynamic Analyses of Composite Beams with Interlayer Slip (Ph.D. thesis), University of Miskolc, 2017.

[42] C. Adam, D. Ladurner, T. Furtmüller, Moderately large deflection of slightly curved layered beams with interlayer slip, Arch. Appl. Mech. accepted for publication (2022).

[43] E. Mettler, in: W. Flügge (Ed.), Dynamic buckling, McGraw-Hill, New York, 1962, 62–1–62–11.

[44] F. Ziegler, Mechanics of Solids and Fluids, second ed., Springer New York, 1995.

[45] Y. Fung, Foundations of Solid Mechanics, Prentice Hall, 1965.

[46] C. Adam, R. Heuer, A. Jeschko, Flexural vibrations of elastic composite beams with interlayer slip, Acta Mech. 125 (1) (1997) 17–30, http://dx.doi.org/10.1007/BF01177296.

[47] R.W. Clough, J. Penzien, Dynamics of Structures, third ed., Computers & Structures Inc., 1995.

[48] Abaqus FEA V. 6.21-6, Simulia (Dassault Systèmes), 2021.

[49] C.W. Bert, M. Malik, Differential quadrature method in computational mechanics: A review, Appl. Mech. Rev. 49 (1) (1996) 1–28, http://dx.doi.org/10.1115/1.3101882, arXiv:https://asmedigitalcollection.asme.org/appliedmechanicsreviews/article-pdf/49/1/1/5437399/1_1.pdf.

[50] Mathematica Version 12.3.1, Wolfram Research, Inc., 2021.

[51] Maple 2021, maplesoft, A division of Waterloo Inc., Waterloo, Ontario, 2021.